# Pattern Formation in Dissipative Nonvariational Systems: The Effects of Front Bifurcations

Aric Hagberg

*Program in Applied Mathematics*
*University of Arizona*
*Tucson, AZ 85721*

Ehud Meron

*Arizona Center for Mathematical Sciences*
*and Department of Mathematics*
*University of Arizona*
*Tucson, AZ 85721*

*Abstract*

Patterns in reaction-diffusion systems often contain two spatial scales; a long scale determined by a typical wavelength or domain size, and a short scale pertaining to front structures separating different domains. Such patterns naturally develop in bistable and excitable systems, but may also appear far beyond Hopf and Turing bifurcations. The global behavior of domain patterns strongly depends on the fronts' inner structures. In this paper we study a symmetry breaking front bifurcation expected to occur in a wide class of reaction-diffusion systems, and the effects it has on pattern formation and pattern dynamics. We extend previous works on this type of front bifurcation and clarify the relations among them. We show that the appearance of front multiplicity beyond the bifurcation point allows the formation of persistent patterns rather than transient ones. In a different parameter regime, we find that the front bifurcation outlines a transition from oscillating (or breathing) patterns to traveling ones. Near a boundary we find that fronts beyond the bifurcation can reflect, while those below it either bind to the boundary or disappear.

## 1. Introduction

Pattern formation out of equilibrium can often be attributed to the coupling of diffusion with local nonlinear dynamics. These processes are explicit in reaction-diffusion systems such as chemical reactions or electrical activation of biological membranes, and implicit in systems whose large scale behavior is governed by dissipative amplitude equations such as lasers. The coupling of nonlinearity and diffusion is most beautifully realized in two chemical systems; the Belousov-Zhabotinsky (BZ) reaction, where a variety of traveling patterns have been observed (for a recent review see [Mer92]), and the Chlorite-Iodide-Malonic-Acid (CIMA) reaction, where stationary, traveling, and turbulent patterns have been found [CDB90,OuS91,LKE92]. Reaction-diffusion systems can be divided into three main categories: Excitable, bistable, and Hopf-Turing systems. Patterns in excitable and bistable systems normally involve front structures separating domains of different uniform or quasi-uniform states. They coexist with one or two stable uniform states and thus need to be triggered by specific choices of initial conditions. A Hopf-Turing system, on the other hand, gives rise to patterns through the destabilization of a uniform stationary state in a Hopf or a Turing bifurcation [Tur52,Mur89]. Close to onset, smooth oscillatory or stationary patterns usually appear. However, as the system is driven away from onset, short scale structures, in the form of boundary layers or fronts, may develop. In this regime, the patterns that emerge resememble those in excitable and bistable systems.

In this paper we study patterns in reaction-diffusion systems consisting of fronts separating different domains. Our primary concern here is with the effect *front bifurcations* may have on the dynamics of fronts and on the patterns they form. Most of our analysis will focus on bistable systems, however, many of the results to be derived also apply to excitable systems, and to Hopf-Turing systems far beyond onset.

We shall consider a specific reaction-diffusion model that exhibits the same variety of patterns that have been observed in both the BZ and CIMA reactions. It shares many gross features with models of the BZ reaction [Fib85] and the Lengyel-Epstein model of the CIMA reaction [LeE92], but is more amenable to analysis. The model consists of two scalar fields, $u(x,t)$ and $v(x,t)$ and contains four parameters; the ratio, $\epsilon = T_u/T_v$, between the time scales associated with the two fields, the ratio, $\delta = D_v/D_u$, between the two diffusion constants, and two parameters, $a_1 > 0$ and $a_0$, characterizing the local reaction dynamics. The model reads

$$u_t = u - u^3 - v + u_{xx}, \tag{1.1a}$$

$$v_t = \epsilon(u - a_1 v - a_0) + \delta v_{xx}, \tag{1.1b}$$

where the subscripts on $u$ and $v$ denote partial derivatives. Models of this type have extensively been studied in the context of excitable media where $\epsilon \ll 1$. The form with $\delta = 0$ is known as the FitzHugh Nagumo model of nerve conduction [Fit61,NAY62]. In the following we will refer to (1.1) as the FitzHugh Nagumo (FHN) model for $\delta \neq 0$ as well.

The stationary homogeneous states of (1.1) are determined by the intersection points of the two nullclines $v = u - u^3$ and $v = (u - a_0)/a_1$. Three basic cases, corresponding to the three types of reaction-diffusion systems mentioned above, can be distinguished as Figs. 1 illustrate. (*i*) The nullclines intersect at a single point lying on one of the outer branches of the cubic nullcline $v = u - u^3$ (Fig. 1*a*). (*ii*) The nullclines intersect at a single point lying on the middle branch of the cubic nullcline (Fig. 1*b*). (*iii*) The nullclines intersect at three points each lying on a different branch of the cubic nullcline (Fig. 1*c*). Note that these intersection points, and consequently the stationary homogeneous states of (1.1), are independent of the parameters $\epsilon$ and $\delta$. These parameters, however, do affect the stability of the stationary homogeneous states, and will serve in the following as bifurcation parameters. They also have physical meanings that do not depend on the details of the FHN model. Thus, with appropriate choices of $\epsilon$ and $\delta$, case (*i*) can describe an excitable medium, case (*ii*) a medium undergoing either an Hopf or a Turing bifurcation, and case (*iii*) a bistable medium. Note also that when $a_0 = 0$, Eqs. (1.1) have an odd symmetry $(u, v) \to (-u, -v)$. Analyzing the symmetric system will help us identifying symmetry breaking bifurcations and multiplicity of stable front solutions. Finally, a few words about notations. The solutions $u(x, t)$ and $v(x, t)$ of (1.1) obviously depend on the four parameters, $a_0$, $a_1$, $\epsilon$, and $\delta$, but we will avoid displaying this dependence unless we specifically wish to address it. In that case we will display only the parameter(s) under consideration (see for example (3.25)). The same rule holds for critical values of $\epsilon$ or $\delta$ at which bifurcations occur (see (3.33)).

We begin in section 2 by first identifying Hopf and Turing bifurcations for case (*ii*). We then use singular perturbation considerations to argue that far beyond these instabilities front structures can develop, and that these structures coincide, to leading order, with the single front solutions of case (*iii*). This will allow, later on, extending some of the conclusions we draw for bistable systems to Hopf-Turing systems driven far beyond onset. In section 3 we proceed to case (*iii*) or bistable systems and study a symmetry breaking front bifurcation that gives rise to front multiplicity. This bifurcation is closely related to chiral symmetry breaking in magnetic domain walls [LaN79] and in front structures arising in forced oscillatory systems [CLH90]. Indeed, some of the results to be derived here apply to these systems as well. The apearance of front multiplicity has dramatic effects on the behavior of patterns. For $\delta$ sufficiently small it allows for the formation of

persistent patterns (stable traveling waves) rather than transient ones, whereas for $\delta$ large enough it is responsible for transitions from oscillating or stationary domains to traveling ones. Another consequence of the coexistence of multiple fronts is the possible reflection of traveling fronts at boundaries. We study these effects in section 4. In section 5 we describe the numerical procedures we have used in our simulations. We conclude in section 6 with a brief summary and a discussion of new problems motivated by the present work.

## 2. The Development of Fronts Far Beyond Onset

The FHN model, like a number of other reaction-diffusion models [RoM92], may undergo both Turing and Hopf bifurcations. Figs. 2 show the patterns that develop near and far from the onset of these instabilities. The appearance of patterns involving two spatial scales far beyond onset can be understood using singular perturbation theory as we now show.

For the sake of simplicity, consider the symmetric FHN model, that is (1.1) with $a_0 = 0$, and assume further that $0 < a_1 < 1$. These parameter settings imply case (*ii*) (see Fig. 1*b*). The stationary homogeneous state, $(u, v) = (0, 0)$, loses stability in a Turing bifurcation when

$$\mu^{-1} = \mu_{tu}^{-1} = 2 - a_1 + 2(1 - a_1)^{1/2}, \quad \text{and} \quad \epsilon > 1/a_1, \tag{2.1}$$

where

$$\mu = \epsilon/\delta.$$

For $\mu^{-1} > \mu_{tu}^{-1}$ the stationary homogeneous state becomes unstable to perturbations of finite wavenumbers. The same state loses stability in a Hopf bifurcation when

$$\epsilon = \epsilon_H = 1/a_1. \tag{2.2}$$

For $\epsilon < \epsilon_H$ it becomes unstable to uniform perturbations.

Far beyond the Turing bifurcation $\mu = \epsilon/\delta \ll 1$. Introducing a rescaled space coordinate $z = \sqrt{\mu}x$, we find that stationary solutions of (1.1) should satisfy

$$\mu u_{zz} + u - v - u^3 = 0, \tag{2.3a}$$

$$v_{zz} + u - a_1 v = 0. \tag{2.3b}$$

In all regions where $u$ varies on the same scale as $v$ we can neglect the second derivative term in (2.3*a*) and solve the remaining cubic equation for $u$ in terms of $v$. There are three

solution branches of which the outer two, $u = u_-(v)$ and $u = u_+(v)$, represent, respectively, low and high $u$ values. In the following we will call regions of high and low $u$ values up state and down state domains, respectively. Using $u_\pm(v)$ in (2.3$b$) we obtain closed equations for $v$ in the up and down state domains. There also might be regions where the second derivative term in (2.3$a$) balances the remaining terms. In these regions $u$ varies on a scale of order $\sqrt{\mu}$ which is much shorter than the scale of order unity over which $v$ varies. Such boundary layers arise when nearby regions converge to different branches $u_\pm(v)$ (because of appropriate initial conditions). Stretching back the space coordinate we find to leading order:

$$u_{xx} + u - v - u^3 = 0 \qquad\qquad v_{xx} = 0. \tag{2.4}$$

These equations have two symmetric *front* solutions

$$v = 0, \qquad\qquad u = \pm \tanh(x/\sqrt{2}). \tag{2.5}$$

To construct approximate solutions representing periodic arrays of front structures as in Fig. 2$b$, we solve the closed equations for $v$ in the up and down state domains, $v_{zz} + u_\pm(v) - a_1 v = 0$, and match the solutions and their first derivatives at the front regions. For short wavelength patterns we may simplify the equations for $v$ by linearizing $u_\pm(v)$ around $v = 0$: $u_\pm(v) \approx \pm 1 - v/2$. Carrying out this calculation we find a band of periodic stationary solutions with up and down state domains of equal size, a consequence of the odd symmetry of the model when $a_0 = 0$. For more details about this type of calculation the reader is referred to Refs. [DKT88,KeL89,Mer92] as well as to Appendix B, where the size of a single domain structure in an asymmetric bistable system is calculated.

Similar considerations apply to the Hopf bifurcation case. Far beyond that bifurcation $\epsilon \ll \epsilon_H$, or $\epsilon \ll 1$ if we choose $a_1 \sim \mathcal{O}(1)$. Traveling wave solutions of (1.1) satisfy

$$\epsilon u_{\zeta\zeta} + \epsilon c_0 u_\zeta + u - v - u^3 = 0, \tag{2.6a}$$

$$\delta v_{\zeta\zeta} + c_0 v_\zeta + u - a_1 v = 0, \tag{2.6b}$$

where $\zeta := \sqrt{\epsilon}(x - ct)$ and $c = c_0\sqrt{\epsilon}$ is the traveling wave speed. This choice of $c$ is appropriate for short wavelength patterns [DKT88], but other choices may work as well [Fif85]. As before, we distinguish between domains where both $u$ and $v$ vary on a scale of order unity, and fronts where $u$ varies on a scale much shorter than that of $v$, this time of order $\sqrt{\epsilon}$. For domains we find again the relations, $u = u_\pm(v)$, and obtain the closed equations for $v$: $\delta v_{\zeta\zeta} + c_0 v_\zeta + u_\pm(v) - a_1 v = 0$. To study the fronts we stretch the moving coordinate frame, $\chi = \zeta/\sqrt{\epsilon} = x - ct$, and find the leading order equations

$$u_{\chi\chi} + c u_\chi + u - v - u^3 = 0 \qquad\qquad \delta v_{\chi\chi} + c v_\chi = 0. \tag{2.7}$$

These equations have the front solution

$$v = v_f, \qquad u = [u_-(v_f)e^{q\chi} + u_+(v_f)]/[1 + e^{q\chi}], \tag{2.8}$$

where $q = [u_+(v_f) - u_-(v_f)]/\sqrt{2}$ and $v_f$ is the (approximately) constant value of $v$ across the front. A symmetric front solution is obtained from (2.8) by the transformation $x \to -x$. Periodic traveling solutions as appear in Fig. 2*d* can be constructed as before.

Note that the singular perturbation analysis sketched above does not depend on the parameter $a_1$ in any way that would affect the qualitative results (at least for patterns whose wavelengths are sufficiently short). In fact, for the particular model considered here, the front structures are strictly independent of $a_1$ (see (2.5,8)). We therefore expect to find similar patterns in bistable systems for which $a_1 > 1$.

## 3. A Front Bifurcation

Despite the vast literature on FHN type models very few studies addressed other than small $\epsilon$ values. The significance of broadening the range of $\epsilon$ is that there exists a critical value $\epsilon_c$ at which a front bifurcation occurs. This bifurcation has important implications on pattern formation as we will see in sections 4 and 5. Rinzel and Terman [RiT82], who studied the FHN model with $\delta = 0$, were the first to observe the creation of fronts at a critical $\epsilon$ value. More recently, Ikeda *et al.* [IMN89] analyzed the regime $\delta/\epsilon \gg 1$, and found a pitchfork front bifurcation. In this section we extend these results in a number of ways. First, we study the FHN model with $\delta = 0$ and obtain explicit forms for the front solutions and for the bifurcation diagram in the vicinity of the bifurcation point. Then we consider nonzero $\delta$ values and evaluate a bifurcation line, $\delta = \delta_c(\epsilon)$, in the $\epsilon - \delta$ plane. Finally, we connect these results to a recent work by Coullet *et al.* [CLH90] where a nonequilibrium analog of the transition from Ising to Bloch walls in ferromagnets with weak anisotropy [LaN79] has been found. This relation gives a broader perspective to the body of works on patterns in FHN type models. Before embarking on the front bifurcation analysis we discuss a few limiting cases of (1.1) which motivate some aspects we wish to emphasize later on.

### 3.1 The variational case: $\epsilon = 0$

The simplest front structures appearing in dissipative systems are those involving a single scalar field. One example, known in the context of equilibrium phase transitions, is the time dependent Ginzburg-Landau (TDGL) model obtained from (1.1) by either setting $\epsilon = 0$, or regarding $v$ to be a constant parameter:

$$u_t = u - u^3 - v + u_{xx}. \tag{3.1}$$

This equation has the variational form

$$u_t = -\delta\mathcal{F}/\delta u, \tag{3.2}$$

where $\mathcal{F}$ is a Lyapunov functional given by

$$\mathcal{F} = \int \big[\mathcal{E}(u,v) + u_x^2/2\big]dx, \qquad \mathcal{E}(u,v) = -u^2/2 + u^4/4 + vu. \tag{3.3}$$

In the terminology of equilibrium phase transitions, $u$ is an order parameter, $v$ is an external field, and $\mathcal{F}$ is a free energy. For $v$ values in the range $-2/(3\sqrt{3}) < v < 2/(3\sqrt{3})$ the free energy density, $\mathcal{E}$, has double-well forms as shown in Figs. 3. The two wells correspond to the stationary homogeneous states, $u_-(v)$ and $u_+(v)$, that solve the cubic equation $u^3 - u + v = 0$.

Front solutions of (3.1) (or domain walls separating different phases) propagate in a preferred direction dictated by the minimization of $\mathcal{F}$. The speed of propagation, $c$, is determined by the nonlinear eigenvalue problem

$$u'' + cu' + u - v - u^3 = 0, \tag{3.4a}$$

$$u(\chi) = \begin{cases} u_+(v) & \chi \to -\infty \\ u_-(v) & \chi \to \infty, \end{cases} \tag{3.4b}$$

where $\chi = x - ct$. An expression for $c$ can be obtained by multiplying (3.4$a$) by $u'$ and integrating along the whole line. This yields

$$c = c(v) = \alpha(v)\Big[\mathcal{E}\big(u_-(v)\big) - \mathcal{E}\big(u_+(v)\big)\Big], \tag{3.5}$$

where $\alpha(v) = 1/\int_{-\infty}^{\infty} u'(v)^2 d\chi$ is positive. For $v = 0$ the two wells of $\mathcal{E}$ are of equal depth and the front solution of (3.4) is stationary ($c = 0$). For negative $v$ values, $\mathcal{E}(u_-) > \mathcal{E}(u_+)$ and the front moves in the positive $x$ direction ($c > 0$) so as to increase that part of the system having lower energy. When $v$ is positive the front propagates toward negative $x$ values ($c < 0$). The explicit form of this front solution is given in (2.8). The symmetric solution is obtained by the transformation $\chi \to -\chi$ and $c \to -c$.

### 3.2 The regime $\epsilon \gg 1$

We turn now to the full form of (1.1) with $\delta = 0$, and study the case of bistability (*iii*) for large $\epsilon$. We denote the two stable, stationary homogeneous states by $(u_\pm, v_\pm)$, where the subscripts $+(-)$ refer to high (low) $u$ and $v$ values (see Fig. 1$c$), and ask what types of fronts connect these two states.

In the regime of large $\epsilon$, the field $v$ varies on a time scale much shorter than that of $u$, at least initially. Stretching the time coordinate by the factor $\epsilon$, we find

$$u_\tau = \nu(u - u^3 - v + u_{xx}), \tag{3.6a}$$

$$v_\tau = u - a_1 v - a_0, \tag{3.6b}$$

where $\nu = \epsilon^{-1} \ll 1$ and $\tau = t/\nu$. On that new scale, the leading order form of $u$ is independent of $\tau$ (set $\nu = 0$ in (3.6$a$)) and equation (3.6$b$) can be solved for $v$:

$$v(x,t) = v_0(x)e^{-\epsilon a_1 t} + a_1^{-1}[u(x,t) - a_0][1 - e^{-\epsilon a_1 t}]. \tag{3.7}$$

Equation (3.7) implies that apart from a short transient of duration $t \sim \mathcal{O}(\epsilon^{-1})$, the $v$ field follows adiabatically the $u$ field: $v = (u - a_0)/a_1$. Using this form in (3.6$a$) or (1.1$a$) we obtain the asymptotic system

$$u_t = (1 - a_1^{-1})u - u^3 - a_0 a_1^{-1} + u_{xx}, \tag{3.8a}$$

$$v = (u - a_0)/a_1. \tag{3.8b}$$

Equation (3.8$a$) has the same variational structure as (3.1) has, and consequently, all the properties discussed in section 3.1 apply here as well. In particular, the property of fronts propagating in the direction dictated by the minimization of the free energy is retained. Note that the original system (1.1) is not variational, but reduces to a variational one in the large $\epsilon$ regime.

### 3.3 The regime $0 < \epsilon \ll 1$

The regime of small $\epsilon$ has been studied extensively (see the reviews [TyK88,Mer92]). The question we address here is how front solutions connecting the two states $(u_\pm, v_\pm)$ differ from those we found for $\epsilon \gg 1$.

Note first that for $\epsilon \ll 1$ the $v$ field remains approximately constant on the length scale over which $u$ varies. Thus, in the narrow front region equation (3.1) applies with $v = v_f$, the value of $v$ at the front position. The front speed is then determined by $c = c(v_f)$ where $c(v)$ is given by (3.5). Imagine now that we prepare the system in the down state $(u_-, v_-)$ and perturb it locally at the left edge of the system so as to induce a transition to the upper branch $u = u_+(v)$. This transition occurs at $v = v_-$ and, as a result, a front propagating to the right, $c = c(v_-) > 0$, will be induced as Fig. 4$a$ demonstrates. If, on the other hand, the system is prepared in the up state $(u_+, v_+)$ and perturbed on the right edge so as to induce a transition to the lower branch $u = u_-(v)$, a front propagating to

the left, $c = c(v_+) < 0$, will be induced as shown in Fig. 4*b*. Once the system is on a given branch it converges to the stationary homogeneous state lying on that branch. The two fronts therefore connect the same asymptotic states as $\chi \to \pm\infty$, but propagate in *opposite* directions. This property of (1.1) reflects its nonvariational structure. Multiplicity of front solutions in reaction-diffusion systems with multiple time scales was first observed by Ortoleva and Ross [OrR75]. The stability of this type of solutions has been proved later by Rinzel and Terman [RiT82]. Note in this respect that the front solution of (3.8), calculated for $\epsilon \gg 1$, is independent of $\epsilon$ and therefore continues to exist for $\epsilon \ll 1$ as well. In this regime, however, it is no longer stable.

The picture revealed so far is as follows: For $\epsilon \gg 1$ there exists only one front solution having the asymptotic behavior $(u, v) \to (u_\pm, v_\pm)$ as $\chi \to \mp\infty$. For $\epsilon \ll 1$ three such front solutions coexist, two of which are stable. In the next section we study the intermediate $\epsilon$ regime where we expect to find a bifurcation from a single to multiple front solutions.

### 3.4 The front bifurcation

We consider the symmetric case ($a_0 = 0$) for which front solutions of (3.8) are stationary. In the following we will always assume the asymptotic behavior, $(u, v) \to (u_\pm, v_\pm)$ as $\chi \to \mp\infty$, unless we specifically mention otherwise. The explicit form of the stationary front solution of (3.8) is (see (2.8))

$$u_s(x) = -u_+ \tanh(\eta x), \qquad v_s(x) = a_1^{-1} u_s(x), \tag{3.9}$$

where $u_+ = -u_- = \sqrt{(}1 - a_1^{-1})$, and $\eta = u_+/\sqrt{2}$. We assume that at some $\epsilon = \epsilon_c$ propagating front solutions, $u = u_p(\chi), \quad v = v_p(\chi)$, where $\chi = x - ct$, bifurcate from (3.9). In the vicinity of the bifurcation point we can expand a propagating front solution in powers of its speed $c$:

$$\begin{aligned} u_p(\chi) &= u_s(\chi) + c u_1(\chi) + c^2 u_2(\chi) + ... \\ v_p(\chi) &= v_s(\chi) + c v_1(\chi) + c^2 v_2(\chi) + ..., \end{aligned} \tag{3.10}$$

as well as $\epsilon$:

$$\epsilon = \epsilon_c + c\epsilon_1 + c^2 \epsilon_2 + .... \tag{3.11}$$

We insert these expansions into the propagating front equations

$$\begin{aligned} u_p'' + c u_p' + u_p - v_p - u_p^3 &= 0 \\ c v_p' + \epsilon(u_p - a_1 v_p) &= 0, \end{aligned} \tag{3.12}$$

collect all terms that contribute to a given order, and solve the resulting equations for the corrections $u_i$'s and $v_i$'s successively as described below. Note that the corrections to

all orders should decay to zero as $\chi \to \pm\infty$ because the leading order form, that is the stationary solution, already satisfies the correct asymptotic limits.

At order $c$ we obtain:

$$\mathcal{M}u_1 = \Big(\frac{1}{\epsilon_c a_1^2} - 1\Big)u_s', \qquad\qquad v_1 = a_1^{-1}u_1 + u_s', \tag{3.13}$$

where $\mathcal{M}$ is the linear operator

$$\mathcal{M} = d^2/d\chi^2 + 1 - a_1^{-1} - 3u_s^2. \tag{3.14}$$

We consider a space of functions that decay to zero as $\chi \to \pm\infty$ (e.g. Schwartz space). On this space $\mathcal{M}$ is self adjoint and has the null vector $u_s'$:

$$\mathcal{M}u_s' = \mathcal{M}^\dagger u_s' = 0. \tag{3.15}$$

Solvability of (3.13) then yields $\epsilon_c = a_1^{-2}$. Using that result in (3.13$a$) we find $\mathcal{M}u_1 = 0$ and thus $u_1 = bu_s'$, where $b$ is arbitrary constant. Note, however, that $u_s'$ is a translation mode and that assigning a particular value to $b$ defines the origin on the $\chi$ axis. For simplicity we choose $b = 0$ and thus obtain

$$u_1 = 0, \qquad\qquad v_1 = u_s'. \tag{3.16}$$

At order $c^2$ we obtain:

$$\mathcal{M}u_2 = -\epsilon_1 a_1^2 u_s' + a_1 u_s'', \qquad\qquad v_2 = a_1^{-1}u_2 + a_1 u_s''. \tag{3.17}$$

Since $u_s$ is odd, solvability of (3.17) requires $\epsilon_1 = 0$. Using that result in (3.17) we find

$$u_2 = \frac{a_1}{2}\chi u_s', \qquad\qquad v_2 = \frac{1}{2}\chi u_s' + a_1 u_s''. \tag{3.18}$$

At order $c^3$ we obtain:

$$\mathcal{M}u_3 = a_1^2 u_s''' - \epsilon_2 a_1^2 u_s', \tag{3.19}$$

which yields the solvability condition $\epsilon_2 = -\frac{2}{5}(1 - a_1^{-1})$.

Summing up these results we obtain

$$\begin{aligned} u_p(\chi) &= u_s + \frac{1}{2}c^2 a_1 \chi u_s' + ... \\ v_p(\chi) &= a_1^{-1}u_s + cu_s' + c^2\Big(\frac{1}{2}\chi u_s' + a_1 u_s''\Big) + ..., \end{aligned} \tag{3.20}$$

and

$$\epsilon = \epsilon_c + \epsilon_2 c^2 + ..., \qquad \epsilon_c = a_1^{-2} \qquad \epsilon_2 = -2(1 - a_1^{-1})/5. \tag{3.21}$$

We verified these results by comparing the pitchfork bifurcation implied by (3.21) with a numerically computed one. The comparison is shown in Fig. 5*a* and indicates good agreement up to speed values $c \sim \mathcal{O}(10^{-1})$. Note that for the bistable case considered here $a_1 > 1$ and consequently $\epsilon_2$ is negative. This ensures that the bifurcation is supercritical.

It is instructive to look at the propagating solutions (3.20) up to corrections of order $c$ (including). These can be written as

$$u_p(\chi) \approx u_s(\chi), \qquad v_p(\chi) \approx a_1^{-1} u_s(\chi + c a_1). \tag{3.22}$$

Comparing with (3.9) we see that, to that order, the solutions for $u$ and $v$ remain the same except that $v$ is *translated* with respect to $u$ by amount proportional to the speed $c$. The direction of translation determines the direction of propagation as Figs. 6 demonstrate. This symmetry breaking is also reflected by the phase portraits of the front solutions in the $u - v$ plane, as Fig. 7 shows. The stationary solution is described by a straight line, $v - a_1^{-1} u = 0$, that does not break the odd symmetry of (1.1) (with $a_0 = 0$), while the propagating solutions break the odd symmetry and deviate from that line. This deviation is related to the front speed through

$$c = \alpha_s \int_{-\infty}^{\infty} (v_p - a_1^{-1} u_p) u_s' d\chi,$$

where $\alpha_s = 1/\int_{-\infty}^{\infty} (u_s')^2 d\chi$.

So far we have considered the symmetric model. In general the parameter $a_0$ will not be zero, unless there exists an inherent symmetry in the system that enforces that condition. When $a_0 \neq 0$ the pitchfork front bifurcation unfolds into a saddle-node bifurcation as the bifurcation diagram shown in Fig. 5*b* suggests. The saddle-node bifurcation occurs at a critical value, $\epsilon_c(a_0)$, smaller than $\epsilon_c = a_1^{-2}$.

### 3.5 Ising vs. Bloch fronts

An interesting distinction between the stationary and the propagating front solutions in the symmetric model can be made once we define an angle or phase in the $u - v$ plane, $\varphi = \arctan(v/u)$. Across the stationary front the phase is constant except at the core where it suffers a jump by $\pi$ and the norm $(u^2 + v^2)^{1/2}$ vanishes. Across a propagating front, on the other hand, the phase rotates smoothly by an angle $\pi$ and the norm never vanishes. An analogous front bifurcation has been found recently by Coullet *et al.* [CLH90] in the forced complex Ginzburg-Landau (CGL) equation

$$A_t = (\rho + i\theta) A + (1 + i\alpha) A_{xx} - (1 + i\beta) |A|^2 A + \gamma \bar{A}, \tag{3.23}$$

where $A(x,t)$ is a complex field. This equation describes spatiotemporal modulations of an oscillating medium, periodically forced at twice the oscillation frequency with strength $\gamma$. The effect of the forcing is to create two stable, phased locked states whose phases, or $\arg(A)$ values, differ by $\pi$. The phase $\arg(A)$ plays the same role as $\varphi$ does in the FHN model; it remains constant or smoothly rotates across a front separating different phase locked states for sufficiently large or small $\gamma$ values, respectively. Coullet *et al.* [CLH90] proposed these types of fronts solutions to be the nonequilibrium analogs of Ising and Bloch walls in ferromagnets with weak anisotropy (where $\arg(A)$ corresponds to the angle the magnetization vector makes with an easy magnetization direction) [LaN79]. In the following we will occasionally follow this terminology and refer to the two types of fronts in the FHN model as Ising and Bloch fronts.

### 3.6 The bifurcation line in the $\epsilon - \delta$ plane

The extension of the bifurcation analysis of section 3.4 to nonzero $\delta$ values is rather tedious and we evaluate here the bifurcation line only. Even this calculation is not simple as the exact stationary front solution is not known. We therefore consider the regime of small $\delta$ values where the stationary front solution can be expanded in powers of $\delta$, and evaluate a linear approximation for the bifurcation line valid for $\delta \ll 1$. At the other extreme, $\delta/\epsilon \gg 1$, we use a singular perturbation analysis, similar to that of Ikeda *et al.* [IMN89]. The complete bifurcation line is obtained numerically by integrating (1.1) with Neumann boundary conditions.

Consider the symmetric model, that is, (1.1) with $a_0 = 0$. A stationary front solution $u = u_s(x;\delta)$ $v = v_s(x;\delta)$ satisfies

$$u_s'' + u_s - v_s - u_s^3 = 0, \tag{3.24a}$$

$$\delta v_s'' + \epsilon(u_s - a_1 v_s) = 0. \tag{3.24b}$$

Note that in these notations $u = u_s(x;0)$, $v = v_s(x;0)$ is the stationary solution (3.9). For $\delta \ll 1$ we can solve (3.24) perturbatively. Since we shall need the form of the stationary solution on the bifurcation line we set $\epsilon = \epsilon_c(\delta)$ in (3.24*b*). Expanding the stationary solution, $u = u_s(x;\delta)$ $v = v_s(x;\delta)$, and $\epsilon_c(\delta)$ in powers of $\delta$,

$$\begin{aligned} u_s(x;\delta) &= u_s(x;0) + \delta u_1(x) + ..., \\ v_s(x;\delta) &= v_s(x;0) + \delta v_1(x) + ..., \end{aligned} \tag{3.25}$$

$$\epsilon_c(\delta) = a_1^{-2} + \delta\epsilon_{c1} + ..., \tag{3.26}$$

and using these expansions in (3.24) we find at order $\delta$

$$\mathcal{M}u_1(x) = u_s''(x;0), \tag{3.27}$$

$$v_1(x) = a_1^{-1}u_1(x) + u_s''(x;0), \tag{3.28}$$

where $\mathcal{M}$ is given by (3.14) with $u_s = u_s(x;0)$. The solution of (3.27) is $u_1(x) = \frac{1}{2}xu_s'(x;0)$. This, together with (3.28), yields the leading order approximation

$$u_s(x;\delta) = u_s(x;0) + \frac{1}{2}\delta x u_s'(x;0) + ..., \tag{3.29a}$$

$$v_s(x;\delta) = a_1^{-1}u_s(x;0) + \frac{1}{2}\delta a_1^{-1}xu_s'(x;0) + \delta u_s''(x;0) + ..., \tag{3.29b}$$

where $u_s(x;0)$ is given by (3.9).

As before we expand $\epsilon$ and the propagation front solutions in power series in $c$ (see (3.10))

$$\begin{aligned} u_p(\chi;\delta) &= u_s(\chi;\delta) + cu_1(\chi;\delta) + ..., \\ v_p(\chi;\delta) &= v_s(\chi;\delta) + cv_1(\chi;\delta) + ..., \end{aligned} \tag{3.30}$$

$$\epsilon = \epsilon_c(\delta) + c\epsilon_1(\delta) + ..., \tag{3.31}$$

and insert these expansions into (1.1). At order $c$ we obtain

$$\begin{pmatrix} \partial_\chi^2 + 1 - 3u_s^2(\chi;\delta) & -1 \\ \epsilon_c/\delta & \partial_\chi^2 - \epsilon_c a_1/\delta \end{pmatrix} \begin{pmatrix} u_1(\chi;\delta) \\ v_1(\chi;\delta) \end{pmatrix} = \\ - \begin{pmatrix} u_s'(\chi;\delta) \\ v_s'(\chi;\delta)/\delta + \epsilon_1[u_s(\chi;\delta) - a_1 v_s(\chi;\delta)]/\delta \end{pmatrix}. \tag{3.32}$$

Solvability of (3.32) requires the right hand side of this equation to be orthogonal to the vector $(u_s'(\chi;\delta), -\frac{\delta}{\epsilon_c}v_s'(\chi;\delta))^T$. This yields the following equation for the bifurcation line:

$$\epsilon = \epsilon_c(\delta) = \int_{-\infty}^{\infty} v_s'(\chi;\delta)^2 d\chi \Big/ \int_{-\infty}^{\infty} u_s'(\chi;\delta)^2 d\chi. \tag{3.33}$$

Using the leading order approximation (3.29) in (3.33) we find

$$\epsilon_c(\delta) = (1 - b\delta)/a_1^2 \qquad \text{or} \qquad \delta_c(\epsilon) = (1 - a_1^2\epsilon)/b \qquad (\delta \ll 1), \tag{3.34}$$

where $b = 4(a_1 - 1)/5$.

In Appendix A we evaluate the bifurcation line for $\delta/\epsilon \gg 1$ using singular perturbation theory. This approach differs from that presented above in that it uses the smallness of $\epsilon/\delta$ rather than that of the speed. As noted by Ikeda *et al.* [IMN89] it yields approximate

front solutions and bifurcation diagrams valid away from the bifurcation point as well. The price though is the limited validity range along the bifurcation line. Using this approach we obtain

$$\epsilon_c(\delta) = d/\delta, \qquad d = 9/(2a_1 + 1)^3, \tag{3.35}$$

where we took $a_0 = 0$ (symmetric model).

Fig. 8 shows the exact bifurcation line obtained by direct numerical integration of (1.1). The linear approximation for $\delta \ll 1$ and the singular perturbation result (3.35) (valid for $\delta/\epsilon \gg 1$) are shown in solid and dashed lines, respectively. We conclude this section by showing in Figs. 9 typical phase portraits of the front solutions (more precisely, projections thereof on the $(u, v)$ plane) for $\delta$ values of order unity or larger. The outer portraits pertain to the two counter propagating front solutions that exist for $\epsilon < \epsilon_c(\delta)$, whereas the middle one represents the stationary front solution at $\epsilon > \epsilon_c(\delta)$. Note that the field $v$ barely changes across the front. This is a consequence of the smallness of $\epsilon/\delta$ (compare with the corresponding phase portraits shown in Fig. 7 for $\delta = 0$).

## 4. Implications on Pattern Formation

### 4.1 The Emergence of Persistent Patterns

A significant implication of the front bifurcation for $\delta = 0$ or sufficiently small is that it tells us where in parameter space we should expect an initial pattern of domains to decay toward a uniform state and where to develop into a stable traveling wave. Consider first the regime of high $\epsilon$ values, $\epsilon \gg \epsilon_c(a_0)$ (see last paragraph of section 3.4). In this parameter regime the nonvariational system (1.1) reduces to the variational system (3.8). As a result, patterns evolve so as to minimize the appropriate free energy functional. Like in equilibrium phase transitions, up state domains either shrink or expand (depending on the sign of $a_0$) to form the uniform state of lowest free energy. The relaxation toward a uniform state occurs even for the symmetric case ($a_0 = 0$) where an isolated front is stationary. As shown by Kawasaki and Ohta [KaO82] and more recently by Carr and Pego [CaP89], nearby fronts that bound a domain attract and annihilate one another on a time scale $t \sim \exp(\lambda/w)$ where $\lambda$ is the domain size and $w$ is the front width. Thus, domains shrink and disappear, but the relaxation can be extremely slow and unnoticible in practice.

We have found numerically that this qualitative behavior remains unchanged for *all* $\epsilon > \epsilon_c(a_0)$. Fig. 10*a* shows the relaxation of an initial pattern toward a uniform state for $\epsilon/\epsilon_c(a_0) = 1.12$. Fig. 10*b* shows the time evolution of the same initial pattern for $\epsilon/\epsilon_c(a_0) = .72$, that is beyond the bifurcation from Ising to Bloch fronts. In contrast to Fig. 10*a*, here, a stable traveling pattern develops. We explored the transition from

transient to persistent patterns more carefully by integrating equations (1.1) for various $\epsilon$ and $a_0$ values keeping the other parameters constant ($\delta = 0$, $a_1 = 2$). The resulting phase diagram is shown in Fig. 11. The solid (right) curve designates the front bifurcation, $\epsilon = \epsilon_c(a_0)$. To the right of this curve only one front solution $(u, v) \to (u_\pm, v_\pm)$ as $x \to \mp\infty$ exists, and initial patterns decay toward a uniform state. To the left of this curve, three front solutions connecting the same asymptotic states coexist; two stable (Bloch fronts) and one unstable (Ising front). Stable traveling waves, however, appear only beyond a second threshold, $\epsilon_p(a_0)$, given by the dashed (left) curve. Using a numerical continuation method we found that for the symmetric case ($a_0 = 0$) traveling wave solutions do exist for $\epsilon_p < \epsilon < \epsilon_c$, but they are unstable. We did not find such solutions for the nonsymmetric model (i.e. for $\epsilon_p(a_0) < \epsilon < \epsilon_c(a_0)$ with $a_0 \neq 0$).

This dramatic change in the qualitative behavior of patterns can be attributed to two related factors; the appearance of front multiplicity and the appearance of a second independent field. The former makes it possible for domains to travel rather than shrink or expand, whereas the latter affects front interactions so as to bind a trailing front to a leading one. In the rest of this section we elaborate on these two factors in some length.

The multiplicity of front solutions for $\epsilon < \epsilon_c(a_0)$ and the symmetry $x \to -x$ of (1.1) imply that along with a front that transforms the lower state $(u_-, v_-)$ to the upper state $(u_+, v_+)$, there exists another front (hereafter "back") propagating in the *same direction* that transforms the upper state back to the lower one (note that the front and the back represent two different Bloch fronts). A combination of the two, using appropriate initial conditions, can yield a traveling up-state domain. To be concrete, let us assume that the (isolated) trailing front, or back, is faster than the leading front. This situation is attenable with $a_0 < 0$. The fate of the traveling domain as the back approaches the (leading) front depends on the interaction between the two. Unlike the case of Ising fronts where the field $v(x,t)$ is eliminated through the relation $v = (u - a_0)/a_1$ and the interaction is attractive, for $\epsilon < \epsilon_c(a_0)$, $v(x,t)$ is independent of $u(x,t)$ and allows for a repulsive interaction as well.

To see this, let us assume that $\epsilon \ll \epsilon_p$ where $\epsilon_p < \epsilon_c \sim \mathcal{O}(a_1^{-2})$. Then $v$ varies on time and length scales much longer than those of $u$. Just behind the front the value of $v$ is still close to the down state value $v_-$. It approches the up state value, $v_+$, only far behind the front. Since $v$ is approximately constant across the narrow back region, the back speed is determined by the local $v$ value, $v_b$, according to (3.5). When the back is still far behind the front $v_b \approx v_+$, the energy difference $\mathcal{V}\big(u_-(v_+)\big) - \mathcal{E}\big(u_+(v_+)\big)$ is large (see Fig. 3*c*) and the speed high. As it approaches the front, however, $v_b$ decreases, the energy difference becomes smaller and the speed lower. Thus, the back is slowed down (or repelled) by the

field $v$ induced by the front. For $\epsilon$ sufficiently small the back approaches the front speed while it is still far behind the front. At such distances the $u$ field follows adiabatically the slow field $v$ (that is, $u = u_+(v)$) and a stable traveling domain of fixed size is formed (see below). For $\epsilon$ values closer to $\epsilon_c$ the adiabatic elimination of $u$ may not be valid and more complicated interactions are possible. We believe that in this parameter range both repulsive and attractive interactions are significant and suggest that the balance between the two gives the threshold $\epsilon_p$ represented in Fig. 11 by the inner curve. We note though that we have not studied yet this regime in detail and that the above suggestion is not founded yet.

To study the formation of a stable traveling domain of fixed size we assume $\epsilon \ll \epsilon_p$ and use a singular perturbation approach. We first evaluate the slow field $v$ that builds up behind a front propagating at constant speed $c = c(v_-)$. In this region $u = u_+(v)$ and the equation we need to solve is

$$cv' + \epsilon\big(u_+(v) - a_1 v - a_0\big) = 0, \tag{4.1}$$

where $v = v(\chi)$ and $\chi = x - ct$. The boundary conditions are

$$v(\chi_f^0) = v_-, \qquad\qquad v(\chi) \to v_+ \ \text{ as } \ \chi \to -\infty, \tag{4.2}$$

where $\chi_f^0$ is the front position in a frame moving at speed $c$. To simplify (4.1) we take $a_1$ to be sufficiently large so that $|v_-| \sim v_+ \ll 1$. The branches $u_\pm$ can then be linearized:

$$u_\pm(v) = \pm 1 - v/2. \tag{4.3}$$

Using (4.3) in (4.1) and solving for $v$ we obtain

$$v(\chi) = (v_- - v_+)e^{\epsilon\kappa(\chi - \chi_f^0)} + v_+, \qquad \chi \le \chi_f^0, \tag{4.4a}$$

where

$$v_\pm = \frac{\pm 1 - a_0}{a_1 + 1/2}, \qquad\qquad \kappa = \frac{a_1 + 1/2}{c}. \tag{4.4b}$$

A traveling domain of fixed size can be obtained by demanding the front and back speeds to be equal

$$-c(v_b^0) = c(v_-) = c. \tag{4.5}$$

This relation together with (3.5) can be used to evaluate $v_b^0 = v(\chi_b^0)$, the level of $v$ at the back position for a domain of fixed size. The fixed size of an up-state domain can be expressed in terms of $v_b^0$ using (4.4$a$):

$$\lambda = \chi_f^0 - \chi_b^0 = \frac{1}{\epsilon\kappa} \ln\Big(\frac{v_+ - v_-}{v_+ - v_b^0}\Big). \tag{4.6}$$

Note that (4.6) requires $v_b^0 < v_+$ or an isolated back to propagate faster than an isolated front. For $v_b^0 > v_+$ (back slower than front) the $v$ field behind the front can never reach the value $v_b^0$ needed for a back to propagate at the front speed. In this case, an up-state domain expands indefinitely, and a down-state domain of fixed size (referred to as an E-pulse in [RiT82]) becomes feasable. We illustrate these two cases in Figs. 12.

The relaxation toward an up-state domain of fixed size can be derived by writing a back solution in the form

$$u_b(x,t) = u_b^0(\chi - \chi_b) + \epsilon u_b^1(\chi - \chi_b, \epsilon t), \tag{4.7a}$$

$$v_b = v(\chi_b) = v_b^0 + \epsilon v_b^1(\epsilon t), \tag{4.7b}$$

where $u_b^0(\chi)$ solves

$$u_b^{0\prime\prime} + c u_b^{0\prime} + u_b^0 - v_b^0 - {u_b^0}^3 = 0, \tag{4.8a}$$

$$u_b^0(\chi) = \begin{cases} u_-(v_b^0) & \chi \to -\infty \\ u_+(v_b^0) & \chi \to \infty, \end{cases} \tag{4.8b}$$

and

$$\chi_b(\epsilon t) = \chi_b^0 + \tilde{\chi}_b(\epsilon t)$$

is the actual back position. The slow time dependence of $v_b$ is introduced to account for the declining $v$ field at the back position as the latter approaches the front. Using (4.7) in (1.1$a$) we find

$$\partial_\chi^2 u_b^1 + c\partial_\chi u_b^1 + (1 - 3{u_b^0}^2) u_b^1 = v_b^1 - \epsilon^{-1}\dot{\chi}_b \frac{du_b^0}{d\chi}, \tag{4.9}$$

where the dot over $\chi_b$ denotes differentiation with respect to the fast time $t$. Solvability of (4.9) requires the right hand side of to be orthogonal to $\exp(c\chi)du_b^0/d\chi$ or

$$\dot{\chi}_b = \beta\epsilon v_b^1, \tag{4.10}$$

where

$$\beta = \int_{-\infty}^{\infty} \frac{du_b^0}{d\chi} e^{c\chi} d\chi \Big/ \int_{-\infty}^{\infty} \Big(\frac{du_b^0}{d\chi}\Big)^2 e^{c\chi} d\chi$$

is a positive constant.

Equation (4.10) relates the back speed to the level of $v$ at the back position. The latter, in turn, can be related to former through (4.4$a$):

$$\epsilon v_b^1 = v(\chi_b) - v_b^0 = (v_+ - v_b^0)\big(1 - e^{\epsilon\kappa\tilde{\chi}_b}\big). \tag{4.11}$$

Combining (4.10) and (4.11) we obtain an equation of motion for the back:

$$\dot{\tilde{\chi}}_b = \beta(v_+ - v_b^0)\big(1 - e^{\epsilon\kappa\tilde{\chi}_b}\big). \tag{4.12}$$

The linearization of (4.12) about $\tilde{\chi}_b = 0$ (i.e. the fixed size domain) gives the equation

$$\dot{\tilde{\chi}}_b = -\epsilon\kappa\beta(v_+ - v_b^0)\tilde{\chi}_b.$$

Recall that $\epsilon$, $\kappa$ and $\beta$ are all positive and $v_b^0 < v_+$ for a relaxation toward an up-state domain. We therfore conclude that the up-state domain whose size is given by (4.6) is stable to translational perturbations. Note that in the small $\epsilon$ regime considered here the size of a domain is much larger than the front (back) width. Thus, the front and back that bound a domain are approximately isolated (see (4.7$a$). The isolated front solutions, in turn, are marginally stable to translations but stable to other types of perturbations (such as amplitude modulations). We therefore expect the translational perturbations to be the most "dangerous" ones.

A similar approach can be used to study the relaxation of arrays of traveling up-state domains toward periodic traveling waves. The difference with respect to a single domain is that now the leading front of any domain propagates into the slowly decaying $v$ field behind the back ahead of it. As a result, the front speed is not constant; it rather depends on the distance between the front and the leading back. A different kinematical approach, leading to equations of motion expressed in implicit form, has been proposed earlier by Keener [Kee80] in the context of excitable media. We also note that the singular perturbation theory sketched above cannot capture an oscillatory decay toward either of the stationary homogeneous states. Such a decay, can lead to spatial chaos as discussed in refs. [EMS88,Mer92].

So far we have considered the case $\delta = 0$. Similar conclusions hold for small enough $\delta$ values. We conclude this section with a numerical study of the forced CGL equation (3.23) for which $\delta = 1$. We have added to the right hand side of this equation a constant term, $\gamma_0$, to break the symmetry between the two phase locked states (analogous to $a_0$). Such a term appears when the periodic forcing contains a component at the medium's oscillation frequency. We have not explored in detail the $(\gamma, \gamma_0)$ parameter plane, but for fixed $\gamma_0$ we did observe transient patterns for $\gamma$ sufficiently large, stable traveling waves for $\gamma$ sufficiently small, and transient patterns involving traveling domains in a narrow range of intermediate $\gamma$ values. This suggests that the qualitative form of the phase diagram drawn in Fig. 11 is quite general and might apply to any system (with $\delta$ relatively small) undergoing an Ising-Bloch type front bifurcation.

### 4.2 Stationary, Oscillating and Traveling Domains in an Infinite System

When the diffusion of $v$ is fast enough stable stationary domains, rather than transient ones, may develop [EHT84] in the regime of Ising fronts. The formation of this type of

domain for $\delta/\epsilon$ sufficiently large is illustrated in Fig. 13. As the two fronts approach one another the $v$ field, inside the domain bounded by the fronts, developes a narrow lumped structure. The consequent diffusive damping lowers the level of $v$ at the front regions and thus slow them down. The size, $\lambda$, of a single stationary domain is given by

$$\lambda = \varpi(\delta/\epsilon)^{1/2}, \qquad \varpi = -\ln(-a_0)/(a_1 + \frac{1}{2})^{1/2}, \tag{4.13}$$

assuming $\mu = \epsilon/\delta \ll 1$. We derive this result in Appendix B using a singular perturbation approach. Note that the stationary domain size decreases as $\mu^{-1} = \delta/\epsilon$ decreases. Obviously, for such a domain to exist its size should be at least of the order of the front width. This consideration explains the existence of a critical value $\mu_{st}^{-1}$, below which stationary domains do not exist. We note that the transition to stationary patterns beyond $\mu_{st}^{-1}$ does not occur by a Turing bifurcation. We remind the reader that we are considering here case (*iii*) pertaining to bistable systems, and that none of the homogeneous states of the system lose stability at the transition point. The transition line in the $\epsilon - \delta$ plane, $\delta = \mu_{st}^{-1}\epsilon$, does resemble, however, the Turing bifurcation line (2.1).

To study how patterns are affected by the front bifurcation, we begin with a *single* stationary domain in an *infinite medium* and follow that structure as we approach the front bifurcation line. We postpone the discussion of periodic domain patterns to the next section. The results to be described below have been obtained numerically. For more details about the numerical procedures the reader is referred to section 5. Our starting point in the $\epsilon - \delta$ plane lies above the transition to stationary domains, $\delta/\epsilon > \mu_{st}^{-1}$, and far to the right of the front bifurcation line, namely, at $\epsilon$ values significantly larger than $\epsilon_c(\delta)$ (see (3.34) and (3.35)). As $\epsilon$ is decreased (keeping $\delta$ constant) past a critical value, $\epsilon_{br}(\delta)$, the stationary domain loses stability in a Hopf bifurcation, and a breathing like oscillatory motion sets in as shown in Fig. 14*a*. This type of oscillations have first been observed by Koga and Kuramoto [KoK80] and more recently have been studied analytically by Nishiura and Mimura [NiM89] (see also [KeL90], [OIT90]). In the latter study a *finite* medium has been considered and the oscillations were found to persist well below $\epsilon_{br}$ without any indication of a secondary bifurcation. Our findings for a single domain in an infinite medium are different; as $\epsilon$ is further decreased the oscillation amplitude grows, leading eventually to the collapse of the domain and to a uniform down state as Fig. 14*b* illustrates (note that the homogeneous states $(u_\pm, v_\pm)$ remain linearly stable for any $\epsilon$ and $\delta$ values). Similar collapse events have recently been found in a model for a semiconductor etalon [RRH93]. The collapse can be avoided by increasing the size of the domain. This can be achieved by making the system more symmetric, that is, by decreasing $|a_0|$. For

$|a_0|$ sufficiently small oscillating domains have been observed all the way down to the front bifurcation line, $\epsilon = \epsilon_c(\delta)$, but not below it!

The effect of the front bifurcation on the behavior of a single domain structure is demonstrated in Figs. 15*a* and 15*b* corresponding to $\epsilon > \epsilon_c(\delta)$ (Ising fronts) and $\epsilon < \epsilon_c(\delta)$ (Bloch fronts), respectively. In both figures the initial conditions consist of two fronts bounding a wide up-state domain and propagating toward one another. In 15*a* the two fronts set in a stable oscillatory motion, whereas in 15*b* they rebound from one another and leave the system in a uniform up state. We attribute this change of behavior to the appearance of multiple fronts. Above the bifurcation line ($\epsilon > \epsilon_c(\delta)$) there exists only one type of stable front solution, approaching $(u_\pm, v_\pm)$ as $\chi \to \mp\infty$ and propagating to the left (assuming $a_0$ negative), or, the symmetric one, approaching $(u_\mp, v_\mp)$ as $\chi \to \mp\infty$ and propagating to the right. Below the bifurcation ($\epsilon < \epsilon_c(\delta)$), another pair of stable front solutions appear (in addition to the aforementioned one): a front approaching $(u_\pm, v_\pm)$ as $\chi \to \mp\infty$ and propagating to the right, and a front approaching $(u_\mp, v_\mp)$ as $\chi \to \mp\infty$ and propagating to the left. In 15*b* the outward propagating front structures converge to the second pair of stable front solutions and thus proceed with the outward motion indefinitely. In 15*a*, on the other hand, there exist no front solutions that pertain to an outward motion. The only front solutions that exist are those propagating toward one another, and the change in the direction of propagation just reflects the convergence toward these solutions.

Figs. 16 show another numerical experiment where the same parameter settings are used but the initial conditions consist now of two fronts propagating in the same direction. For $\epsilon > \epsilon_c(\delta)$ (Fig. 16*a*), the front on the right side of the domain changes its direction of propagation and an oscillatory motion sets in. For $\epsilon < \epsilon_c(\delta)$ (Fig. 16*b*), a stable *traveling domain*, is obtained.

We note that the stationary domain solution still exists on both sides of the bifurcation line but is unstable. Fig. 17 shows a typical bifurcation diagram for domain structures. It does not capture the oscillatory domain solutions or the collapsing solutions (see section 5) but it shows the destabilization of the stationary domain solution at $\epsilon = \epsilon_{br}$, and how traveling domain solutions bifurcate from it. We also note that by making the system more symmetric (i.e. decreasing $|a_0|$) the destabilization of the stationary domain solution occurs closer to the bifurcation to traveling domains. For sufficiently symmetric systems it might be possible for the stationary domain solution to remain stable all the way down to the traveling-domain branch, but we have not verified that.

A bifurcation from stationary to traveling domain solutions has already been found in the context of excitable media [DoK89]. What is new in our findings is that this transition

is a consequence of the front bifurcation. Indeed, we have verified numerically that the appearance of traveling domain solutions at $\epsilon = \epsilon_{tr}(\delta)$ (see Fig. 17) coincides, within the numerical accuracy, with the front bifurcation line, $\epsilon = \epsilon_c(\delta)$, at least above the onset of stationary domains (the line $\delta = \mu_{st}^{-1}\epsilon$). Well below that line $\epsilon_{tr}$ deviates from $\epsilon_c$ and converges, at $\delta = 0$, to $\epsilon_p$ (see section 4.1).

We summarize the discussion of single domain structures in infinite media by showing in Fig. 18 a phase diagram in the $\epsilon - \delta$ plane. The diagram is divided into four main regions. Region I, $\epsilon > \epsilon_{tr}(\delta)$ and $\epsilon > \mu_{st}\delta$, where domain structures are transient and the asymptotic state is either the uniform up or uniform down state. Region II, $\epsilon > \epsilon_{br}(\delta)$ and $\epsilon < \mu_{st}\delta$, where stationary domains prevails. Region III, $\epsilon > \epsilon_{tr}(\delta)$, $\epsilon < \mu_{st}\delta$, and $\epsilon < \epsilon_{br}(\delta)$, where domains oscillate. And region IV, $\epsilon < \epsilon_{tr}(\delta)$, where domains travel invariably. The hatched area in region III designates, in a schematic manner, the regime of steadily oscillating domains. Outside this regime domains oscillate for a while and then collapse. Depending on the asymmetry of the system, this regime may shrink to a narrow strip below the line $\epsilon = \epsilon_{br}(\delta)$ (strong asymmetry), or span the whole range between the lines $\epsilon = \epsilon_{br}(\delta)$ and $\epsilon = \epsilon_{tr}(\delta)$ (weak asymmetry). The range between the two lines, in turn, becomes smaller the more symmetric is the system. Note the thick solid-dashed line. This is the front bifurcation line ($\epsilon = \epsilon_c(\delta)$) which coincides with the onset of traveling domains at $\epsilon = \epsilon_{tr}(\delta)$ apart from a small portion at small $\delta$ values.

### 4.3 Periodic Domain Patterns

The behavior of periodic domain patterns is similar in many respects to that of single domain structures. One notable difference though is the persistent of stable oscillating domain solutions to the left of the front bifurcation line ($\epsilon < \epsilon_c(\delta)$), where they coexist with stable traveling domain solutions as Figs. 19 demonstrate. The regime of coexistence seems to be limited; far enough from the front bifurcation line we found the traveling domain solutions to prevail. The existence of oscillatory dynamics in the regime of multiple fronts is a consequence of front interactions. As nearby domains expand and approach one another there is little room left for diffusion of $v$. As a result the level of $v$ at any front position increases and the fronts change their directions of propagation.

Another difference between periodic and single domain patterns is the possibility of having various modes of oscillation. Ohta *et al.* [OIT90] have identified three such modes; an in-phase mode where all domains expand and shrink simultaneously, an out-of-phase mode where nearby domains oscillate with a phase shift of $\pi$, and an "acoustic" mode, where nearby domains travel in opposite directions back and forth (note that in the latter case the spaces between the domains, or the down-state domains, undergo out-of-phase

oscillations). Of the three, the in-phase mode is the first to be excited. As pointed out by Ohta *et al.* [OIT90], this can be understood by considering the stabilizing effect the diffusion of $v$ has. The in-phase mode involves uniform deviations of $v$ from the stationary domain profile and stabilization by diffusion does not take place. The out-of-phase mode, on the other hand, pertains to alternating deviations every second front site. In this case diffusion of $v$ tends to smear out these deviations and thus to stabilize the stationary pattern against this mode. Similar considerations hold for the acoustic mode. In the numerical experiments we have conducted the in-phase mode always prevailed, even at relatively small $\delta$ values, where the diffusive damping of that mode is weaker.

We expect Hopf-Turing systems, driven far beyond the Turing instability, to exhibit the same phenomenology that short-wavelength patterns in bistable systems do. Indeed, by decreasing $\epsilon$ at constant $\delta$ (far beyond the Turing instability) we found a transition from stationary to oscillating patterns, followed by a transition to traveling patterns.

### 4.4 Reflection at Boundaries

The front bifurcation may drastically affect the behavior of fronts near an impermeable boundary. The effect of such a boundary is similar to that of another approaching front and the scenario of behaviors is similar to that found for domain structures. Figs. 20 show the boundary effects as we cross all four regions in the $\epsilon - \delta$ plane by decreasing $\epsilon$ at constant $\delta$ (the simulations were carried out with Neumann boundary conditions). In region I (transient domains) the front is absorbed at the boundary, leaving the system in a uniform state. In region II (stationary domains), the front comes to a stop at a characteristic distance from the boundary, whereas in region III (oscillating domains) it oscillates near the boundary. In all these regions the (Ising) front is either absorbed at the boundary or is bound to it. By contrast, in region IV the front is *reflected*. This is a consequence of the coexistence of two counter propagating Bloch fronts beyond the front bifurcation line. At front speeds high enough relative to the diffusion of $v$, both Ising and Bloch fronts are absorbed at the boundaries. Ising fronts, however, never reflect at boundaries.

## 5. Numerical Procedures

Numerical simulations of (1.1) were performed using the method of lines with the spatial derivatives approximated by 2nd or 4th order finite differences on a uniform mesh. To solve the resulting system of ordinary differential equations, we used a stiff ODE solver [NKM89]. This solver implements the implicit methods of Gear [Gea71] with adaptive control of both time step and method order.

For the computations pertaining to single domain structures in inifinite systems the

simulations were done with Neumann (no flux) boundary conditions and large computational system sizes. We checked the results with larger system sizes to ensure that the boundaries did not contribute any measurable effect on the solution. When the simulations pertain to periodic patterns, periodic boundary conditions were applied. Occasionally we used periodic boundary conditions for single traveling domains rather than Neumann boundary conditions (see for example Fig. 16*b*). In those cases we chose the period to be large in comparison with the domain size and checked that the two types of boundary conditions gave the same solution within the numerical accuracy.

For the continuation of solutions we used the bifurcation package AUTO [Doe86]. Starting with a stable traveling or stationary solution computed with our PDE solver we continued a periodic solution in one or two parameters to study the effects of parameter variations on the existence and stablilty of solutions. When AUTO failed to give accurate stability information, due to the approach of the periodic orbit towards two heteroclinic cycles, we used our PDE solver to integrate the computed solution forward in time to check its stability.

To find the oscillating domains region we linearized (1.1) about the numerically computed stationary solution and solved the resulting eigenvalue problem. The spatial part of the linearized operator was discretized using 2nd order finite differences on a nonuniform mesh with grid points concentrated near the steep gradient front structures of the domain. We solved the eigenvalue problem using the IMSL routine DEVCRG for real general matrices. Decreasing $\epsilon$ below the line $\epsilon = \epsilon_{br}(\delta)$ a pair of complex conjugate eigenvalues crosses the imaginary axis indicating that the stationary stable solution goes unstable through a Hopf bifurcation to an oscillating domain.

## 6. Conclusion

We have studied a front bifurcation, likely to occur in a variety of nonvariational reaction diffusion systems, and the possible consequences of this bifurcation on pattern formation and pattern dynamics. The bifurcation is accompanied by the appearance of a second independent field which breaks the odd symmetry of front solutions, and leads to a richer dynamical behavior. The main effect of the bifurcation, regarding patterns, is to allow the formation of stable traveling domain patterns. For small $\delta$ values (including $\delta = 0$), it provides a mechanism for pattern formation as no persistent domain patterns can be formed below the bifurcation. For larger $\delta$ values it is responsible for transitions from transient, oscillating, or stationary patterns to traveling ones. Other consequences of the bifurcation are a coexistence regime of traveling and oscillating patterns, and the possible reflection of fronts at boundaries.

These results were obtained for bistable systems but are also relevant to excitable and Hopf-Turing systems as the latter can be obtained by unfolding the former. In this sense, the variety of chemical-wave phenomena in excitable and oscillatory systems can be regarded as a consequence of an Ising-Bloch front bifurcation occurring nearby in parameter space. A more specific implication for Hopf-Turing systems is the prediction of a transition from stationary to oscillating patterns, and from oscillating to traveling patterns far beyond the Turing instability. These transitions may shed light on the complex spatio-temporal behavior that has recently been observed in the CIMA reaction by Ouyang and Swinney [OuS91].

Beyond these specific results and implications, the present analysis demonstrates the usefulness of focusing attention on localized structures that appear in extended patterns. This view lies behind the various kinematical approaches to pattern dynamics [KiM89,NeM92,Mer92,CrH93], where the effects of small perturbations and weak interactions on the dynamics of localized structures are studied. The point we wish to emphasize here is that it is also important to look for structural changes that localized structures might undergo as these can drastically affect pattern dynamics.

We confined ourselves in this paper to patterns in one space dimension, but we expect the front bifurcation to have important effects in two dimensions as well. Perhaps the first question that needs to be addressed concerns the dynamics of a curved Bloch front near the front bifurcation point. The dynamics of a such a front far beyond the bifurcation is well known [TyK88,Mer92]; the normal speed $c_n$ is affected by the curvature $k$ according to the simple linear law, $c_n = c - Dk$, where $D$ is a positive constant having the dimension of a diffusion coefficient. The consequent effect of curvature is to smooth out any wiggles along the front and thus to stabilize its dynamics. Close to the bifurcation point we expect this relation to be highly nonlinear. This might change the role of curvature in a way that still needs to be explored.

An important consequence of the Ising-Bloch front bifurcation in two space dimensions is the possible formation of spiral waves. As pointed out by Coullet, a spiral wave can be created by joining end to end two counter propagating Bloch fronts. This view goes back to Fife [Fif88] who discussed the twisting action induced by joining a front and a back end to end in an excitable medium. All studies of spiral waves so far have taken $\epsilon$ to be a small parameter, and therefore are only valid far from the front bifurcation. The expected nonlinear relation between curvature and normal speed close to the bifurcation point makes the study of spiral waves in that regime potentially interesting.

**Acknowledgements**

We would like to thank Rob Indik and Jerry Moloney for interesting discussions. We also wish to thank the Arizona Center for Mathematical Sciences (ACMS) for support. ACMS is sponsored by AFOSR contract FQ8671-9000589 (AFOSR-90-0021) with the University Research Initiative Program at the University of Arizona. One of us (A.H.) acknowledges the support of the Computational Science Graduate Fellowship Program of the Office of Scientific Computing in the Department of Energy.

**Appendix A: The front bifurcation for $\epsilon/\delta \ll 1$**

We consider here the regime $\epsilon/\delta \ll 1$ and use singular perturbation theory to derive the front bifurcation line. Rescaling space and time according to

$$z = \sqrt{\mu}x, \qquad \tau = \epsilon t, \qquad \mu = \epsilon/\delta \ll 1,$$

and assuming traveling solutions, $u = u(\zeta)$ and $v = v(\zeta)$, where $\zeta = z - c\tau$, we obtain from (1.1)

$$\begin{aligned} \mu u_{\zeta\zeta} + c\delta\mu u_\zeta + u - u^3 - v = 0 \\ v_{\zeta\zeta} + cv_\zeta + u - a_1 v - a_0 = 0. \end{aligned} \tag{A2}$$

We consider front solutions of (A2) that satisfy $(u, v) \to (u_\pm, v_\pm)$ as $\zeta \to \mp\infty$, and set the origin, $\zeta = 0$, by demanding $u(0) = 0$. Outer solutions of (A2) are obtained by setting $\mu = 0$ and solving

$$v_{\zeta\zeta} + cv_\zeta + u_\pm(v) - a_1 v - a_0 = 0, \tag{A3}$$

for $\zeta < 0$ ($u = u_+(v)$) and $\zeta > 0$ ($u = u_-(v)$). To simplify (A3) we approximate the branches $u_\pm(v)$ by the linear forms (4.3). This approximation can be controlled by varying $a_1$. We then obtain the following boundary value problems:

$$\begin{aligned} v_{\zeta\zeta} + cv_\zeta - k^2 v + k^2 v_+ = 0, \qquad \zeta < 0 \\ v(-\infty) = v_+ \qquad v(0) = v_f, \end{aligned} \tag{A4}$$

and

$$\begin{aligned} v_{\zeta\zeta} + cv_\zeta - k^2 v + k^2 v_- = 0, \qquad \zeta > 0 \\ v(\infty) = v_- \qquad v(0) = v_f, \end{aligned} \tag{A5}$$

where $v_\pm$ are given by (4.4*b*), $k^2 = a_1 + \frac{1}{2}$ and $v_f$ is the level of $v$ at the front position. The solutions are

$$v(\zeta) = (v_f - v_+)e^{\sigma_1\zeta} + v_+, \qquad \zeta < 0, \tag{A6}$$

$$v(\zeta) = (v_f - v_-)e^{\sigma_2\zeta} + v_-, \qquad \zeta > 0, \tag{A7}$$

where

$$\sigma_{1,2} = -c/2 \pm (c^2/4 + k^2)^{1/2}. \tag{A8}$$

Matching the derivatives of the two outer solutions at $\zeta = 0$ yields

$$v_f = -\frac{c}{2k^2(c^2/4 + k^2)^{1/2}} - \frac{a_0}{k^2}. \tag{A9}$$

A second relation between $v_f$ and $c$ is obtained by solving the inner problem. To this end we stretch the traveling-frame coordinate according to $\chi = \zeta/\sqrt{\mu}$ and obtain from $(A2)$

$$\begin{aligned} u_{\chi\chi} + \eta c u_\chi + u - u^3 - v = 0, \\ v_{\chi\chi} + \sqrt{\mu} c v_\chi + \mu(u - a_1 v - a_0) = 0, \end{aligned} \tag{A10}$$

where $\eta^2 = \epsilon\delta$. Setting formally $\mu = 0$ in $(A10)$ we obtain a nonlinear eigenvalue problem for $c$,

$$\begin{aligned} u_{\chi\chi} + \eta c u_\chi + u - u^3 - v_f = 0, \\ u(\mp\infty) = u_\pm(v_f) = \pm 1 - v_f/2, \end{aligned} \tag{A11}$$

which yields the second relation between $v_f$ and $c$:

$$v_f = -\frac{\sqrt{2}}{3}\eta c. \tag{A12}$$

Comparing $(A9)$ and $(A12)$ we find

$$\frac{\sqrt{2}}{3}\eta c = \frac{c}{2k^2(c^2/4 + k^2)^{1/2}} + \frac{a_0}{k^2}. \tag{A13}$$

A plot of the solutions $c = c(\eta)$ of $(A13)$ in the $(c, \eta)$ plane yields a bifurcation diagram with $\eta$ being the bifurcation parameter. Consider now the symmetric case, $a_0 = 0$. Assuming propagating solutions ($c \neq 0$) and taking the limit $c \to 0$ we find the bifurcation point

$$\eta_c = \frac{3}{(2a_1 + 1)^{3/2}},$$

or, recalling that $\eta^2 = \epsilon\delta$, the bifurcation line

$$\delta_c(\epsilon) = \frac{9}{\epsilon(2a_1 + 1)^3}. \tag{A14}$$

**Appendix B: Stationary-Domain Solutions for $\epsilon/\delta \ll 1$**

Stationary-domain solutions of (1) satisfy

$$\begin{aligned} \mu u_{zz} + u - u^3 - v = 0 \\ v_{zz} + u - a_1 v - a_0 = 0, \end{aligned} \tag{B2}$$

where $z = \sqrt{\mu}x$ and $\mu = \epsilon/\delta$ is sufficiently small. In the following we will assume that $\mu \ll 1$ and that $a_0 < 0$. The latter assumption means that an Ising front connecting an up state on the left with a down state on the right propagates to the left and consequently that a single domain is an up-state domain (see Fig. 13). Outer solutions are obtained by setting $\mu = 0$ in (B2). We look for such solutions in three regions, $z < z_l$, $z > z_r$, and $z_l < z < z_r$, where $z_l$ and $z_r$ are the positions of the fronts that bound the stationary domain from the left and the right, respectively. The first two regions pertain to down-state domains in which we need to solve

$$v_{zz} - k^2 v + k^2 v_- = 0, \tag{B2}$$

subject to the boundary conditions

$$\begin{aligned} v(-\infty) = v_- \qquad v(z_l) = v_l \qquad \text{for} \quad z < z_l, \\ v(\infty) = v_- \qquad z(z_r) = v_r \qquad \text{for} \quad z > z_r, \end{aligned} \tag{B3}$$

where $v_l$ and $v_r$ are yet to be determined. The third region, $z_l < z < z_r$, corresponds to an up-state domain in which we solve

$$v_{zz} - k^2 v + k^2 v_+ = 0, \tag{B4}$$

subject to the boundary conditions

$$v(z_l) = v_l \qquad v(z_r) = v_r. \tag{B5}$$

In (B2) and (B4), $k^2 = a_1 + 1/2$ and we have used the linearized forms of the branches $u_\pm(v)$ (see (4.3)).

The solutions of (B2) to (B5) are:

$$v(z) = (v_l - v_-)e^{k(z-z_l)} + v_- \qquad z < z_l, \tag{B6}$$

$$v(z) = (v_r - v_-)e^{-k(z-z_r)} + v_- \qquad z > z_r, \tag{B7}$$

and

$$v(z) = \frac{1}{\sinh(k\Lambda)}\Big[(v_r - v_+)\sinh k(z - z_l) - (v_l - v_+)\sinh k(z - z_r)\Big] + v_+ \qquad z_l < z < z_r, \tag{B8}$$

where $\Lambda = z_r - z_l$. Matching the first derivatives of these solutions at $z = z_l$ and $z = z_r$ we find that $v_l = v_r$ and that $\Lambda$ (the domain width) solves the equation

$$\coth k\Lambda - \mathrm{csch} k\Lambda = (v_r - v_-)/(v_+ - v_r). \tag{B9}$$

Equation ($B9$) still contains one unknown parameter, $v_r$. This parameter is obtained from the analysis of the inner regions centered at $z = z_l$ and $z = z_r$. Stretching the coordinate system according to $x = z/\sqrt{\mu}$ and setting $\mu = 0$ we find

$$u_{xx} + u - u^3 - v_r = 0, \tag{B10}$$

implying $v_r = 0$. Using this result in ($B9$) and solving for $\Lambda$ we get

$$\Lambda = -\frac{1}{k}\ln(-a_0), \tag{B11}$$

or (4.13) where $\lambda = \Lambda/\sqrt{\mu}$.

## References


[CaP89] J. Carr and R. L. Pego 1989 *Comm. Pure and Appl. Math.* **42** 523.

[CDB90] V. Castets, E. Dulos, J. Boissonade and P. De Kepper 1990 *Phys. Rev. Lett.* **64** 2953.

[CLH90] P. Coullet, J. Lega, B. Houchmanzadeh, and J. Lajzerowicz, 1990 *Phys. Rev. Lett.* **65** 1352.

[CrH93] M. C. Cross and P. C. Hohenberg 1993 Pattern Formation Outside of Equilibrium, preprint.

[DKT88] J. D. Dockery, J. P. Keener and J. J. Tyson 1988 *Physica D* **30** 177.

[Doe86] E. J. Doedel 1986 *Software for continuation and bifurcation problems in ordinary differential equations* California Instititue of Technology.

[DoK89] J. D. Dockery and J. P. Keener 1989 *SIAM J. Appl. Math.* **49** 539.

[EHT84] G. B. Ermentrout, S. P. Hastings and W. C. Troy 1984 *SIAM J. Appl. Math.* **42** 219.

[EMS88] C. Elphick, E. Meron and E. A. Spiegel 1988 *Phys. Rev. Lett.* **61** 496.

[FiB85] R. J. Field and M. Burger 1985 *Oscillations and Traveling Waves in Chemical Systems* Wiley, New York.

[Fif85] P. C. Fife 1985 *J. Stat. Phys.* **39** 687.

[Fif88] P. C. Fife 1988 *CBMS-NSF Regional Conf. Series in Appl. Math.* **53** 1.

[Gea71] C. W. Gear 1971 *Numerical initial value problems in ordinary differential equations* Prentice-Hall.

[IMN89] H. Ikeda, M. Mimura and Y. Nishiura 1989 *Nonl. Anal. TMA* **13** 507.

[KaO82] K. Kawasaki and T. Ohta 1982 *Physica* **116A** 573.

[Kee80] J. P. Keener 1980 *SIAM J. Appl. Math.* **39** 528.

[KoK80] S. Koga and Y. Kuramoto 1980 *Prog. Theor. Phys.* **63** 106.

[KeL89] D. A. Kessler and H. Levine 1989 *Physica D* **39** 1.

[KeL90] D. A. Kessler and H. Levine 1990 *Phys. Rev. A* **41** 5418.

[KiM89] Y. S. Kivshar and B. A. Malomed 1989 *Rev. Mod. Phys.* **61** 763.

[LaN79] J. Lajzerowicz and J. J. Niez 1979 *J. Phys (Paris) Lett.* **40** L165.

[LeE92] I. Lengyel and I. R. Epstein 1992 *Proc. Natl. Acad. Sci. U.S.A.* **89** 3977.

[LKE92] I. Lengyel, S. Kádàr, and I. R. Epstein 1992 *Phys. Rev. Lett.* **69** 2729.

[Mer92] E. Meron 1992 *Physics Reports* **218** 1.

[Mur89] J. D. Murray 1989 *Mathematical Biology* Springer, New York.

[NeM92] A. C. Newell and J. V. Moloney 1992 *Nonlinear Optics* Addison Wesley (section 3g).

[NiM89] Y. Nishiura and M. Mimura 1989 *SIAM J. Appl. Math.* **49** 481.

[NKM89] S. Nash, D. Kahaner and C. Moler 1989 *Numerical methods and software* Prentice Hall.

[OIT90] T. Ohta, A. Ito and A. Tetsuka 1990 *Phys. Rev. A* **42** 3225.

[OrR75] P. Ortoleva and J. Ross 1975 *J. Chem. Phys.* **63** 3398.

[OuS91] Q. Ouyang, H. L. Swinney 1991 *Chaos* **1** 411.

[RiT82] J. Rinzel and D. Terman 1982 *SIAM J. Appl. Math.* **42** 1111.

[RoM92] A. Rovinsky and M. Menzinger 1992 *Phys. Rev. A* **46** 6315.

[RRH93] U. A. Rzhanov, H. Richardson, A. A. Hagberg, and J. V. Moloney 1993 *Phys. Rev. A* **47** 1480.

[Tur52] A. M. Turing 1952 *Philos. Trans. Roy. Soc. London B* **327** 37.

[TyK88] J. J. Tyson and J. P. Keener 1988 *Physica D* **32** 327.

## Figure Captions

**Figure 1:** Three basic cases for the nullclines of the model system (1.1). Case (i): The nullclines intersect at a single point on an outer branch of the cubic nullcline. Case (ii): The nullclines intersect at a single point on the middle branch of the cubic nullcline. Case (iii): The nullclines intersect at three points each on a different branch of the cubic nullcline.

**Figure 2:** Patterns near and far from onset show the development of two spatial scales. (a) Stationary periodic pattern near onset of the Turing instability. (b) Stationary periodic pattern far from onset of the Turing instability. (c) Traveling pattern near the Hopf bifurcation. (d) Traveling pattern far from the Hopf bifurcation. In all the figures the solid line is the $u$ field and the dashed line is the $v$ field.

**Figure 3:** The free energy density $\mathcal{E}$ (see (3.3)) for different values of $v$.

**Figure 4:** Multiplicity of stable front solutions when $\epsilon \ll 1$. (a) Preparing the system in the down state and perturbing it locally at the left edge of the domain induces a front propagating to the right. (b) Preparing the system in the up state and perturbing it locally at the right edge of the domain induces a front propagating to the left.

**Figure 5:** Bifurcation diagrams of front solutions. The dots are data points representing the speed of the different types of stable front solutions that exist for each value of $\epsilon$. (a) The symmetric case ($a_0 = 0$). The solid line is the theoretical bifurcation diagram computed from (3.21). (b) The nonsymmetric case ($a_0 = .1$) shows the unfolding of the pitchfork to a saddle node bifurcation.

**Figure 6:** The propogation direction of Bloch fronts is determined by the translation of the $v$ field relative to the $u$ field; $v$ always lags behind $u$ unless the front is stationary. (a) Left traveling front. (b) Stationary front. (c) Right traveling front.

**Figure 7:** Phase portraits of front solutions connecting the $(u_+, v_+)$ state at $\chi = -\infty$ to the $(u_-, v_-)$ state at $\chi = \infty$ for the symmetric model ($a_0 = 0$) with $\delta = 0$. The light colored curves are the nullclines $f = 0$ and $g = 0$ and the dark colored curves are the numerically computed trajectories. The trajectory through $(0, 0)$ corresponds to the symmetric stationary front solution. The two other trajectories break the odd symmetry of the system and correspond to traveling fronts. The computational parameters are $\epsilon = 1.0, \delta = 0, a_1 = 2.0, a_0 = 0$ for the stationary front and the same with $\epsilon = .2$ for the two traveling fronts.

**Figure 8:** The front bifurcation line in the $\epsilon - \delta$ plane for the symmetric ($a_0 = 0$) model with $a_1 = 2.0$. The solid circles represent the numerically calculated bifurcation line. The solid line is the linear approximation (valid for $\delta \ll 1$) and the dashed line is the singular

pertubation result (valid for $\delta/\epsilon \gg 1$).

**Figure 9:** Phase portraits of front solutions connecting the $(u_+, v_+)$ state at $\chi = -\infty$ to the $(u_-, v_-)$ state at $\chi = \infty$ for the symmetric model ($a_0 = 0$) with $\delta > 1$. The light colored curves are the nullclines $f = 0$ and $g = 0$ and the dark colored curves are the numerically computed trajectories. The trajectory through $(0, 0)$ corresponds to the symmetric stationary front with $\epsilon > \epsilon_c(\delta)$ and the two other trajectories correspond to the symmetry breaking traveling fronts with $\epsilon < \epsilon_c(\delta)$.

**Figure 10:** (a) Relaxation of an initial pattern to the uniform down state for the regime of Ising fronts, $\epsilon = 0.14, \delta = 0, a_1 = 2.0, a_0 = -0.1$. (b) The convergence of the same initial pattern toward a stable traveling pattern beyond the bifurcation from Ising to Bloch fronts, $\epsilon = 0.09$.

**Figure 11:** Phase diagram in the $\epsilon - a_0$ plane. For the region to the right of the solid curve only one type of front solution exists and initial patterns do not persist. In the region between the solid and the dashed curves multiple stable fronts coexist but patterns still decay toward a uniform state. For the region to the left of the dashed curve initial patterns evolve toward persistent patterns in the form of stable traveling waves. Computational parameters are : $\delta = 0,\ a_1 = 2.0$.

**Figure 12:** Time evolution of a front and a back (or two Bloch fronts following one another). (a) The back propagates faster than the front and binds to the front to form a traveling up state domain. (b) The back propagates slower than the front and the up state domain expands indefinitely.

**Figure 13:** The onset of stationary domains in the Ising front regime as $\delta/\epsilon$ is increased. Ising fronts either (a) collide and anihilate to form a uniform state for $\epsilon > \mu_{st}\delta$, or (b) slow to a stop and form a stationary domain for $\epsilon < \mu_{st}\delta$.

**Figure 14:** Oscillating or breathing domains. (a) Steady oscillations close to the Hopf bifurcation. Computational parameters $\epsilon = 0.03, \delta = 2.5, a_1 = 2.0, a_0 = -0.1$. (b) Collapse of an oscillating domain further away from the Hopf bifurcation. Compuational parameters are the same with $\epsilon = 0.025$.

**Figure 15:** The effect of the front bifurcation on the dynammics of two fronts propagating toward one another: (a) Below the bifurcation ($\epsilon > \epsilon_c(\delta)$ an oscillating domain is formed. Computational parameters: $\epsilon = 0.03, \delta = 2.5, a_1 = 2.0, a_0 = -0.01$. (b) Beyond the bifurcation the two fronts rebound from one another and propagate to the boundaries. Same parameters as in (a) except that $\epsilon = 0.012$.

**Figure 16:** The effect of the front bifurcation on the dynamics of two fronts following one another: (a) Below the bifurcation ($\epsilon > \epsilon_c(\delta)$) an oscillating domain is formed. Computational parameters are $\epsilon = 0.030, \delta = 2.5, a_1 = 2.0, a_0 = -0.012$. (b) Beyond the bifurcation

a traveling domain is formed. Same parameters as in (a) except that $\epsilon = 0.25$.

**Figure 17:** A typical bifurcation diagram for single domain structures. The solutions shown with the solid (dashed) line are stable (unstable) structures. The stationary domain solution loses stability to an oscillating domain at $\epsilon = \epsilon_{br}$. At $\epsilon = \epsilon_{tr}$, a branch of stable traveling domain solutions appears. By the symmetry $c \to -c,\ \chi \to -\chi$, this diagram is symmetric with respect to the $c = 0$ axis, but only the positive speed branch of traveling domain solutions is shown. Also, there is an additional branch of zero speed solutions that is unstable for all values of $\epsilon$. Parameters: $\delta = 2.5, a_1 = 2.0, a_0 = -.1$, period $= 100$.

**Figure 18:** Phase diagram for single domain structures in the $\epsilon - \delta$ plane. In region I, domain structures are transient and the asymptotic state is either the uniform up or down state. In region II stable stationary domains coexist with the uniform up and down states. In region III domains oscillate with a typical region of steady oscillations denoted by the hatched area. In region IV domains travel. The boundary between regions III and IV (i.e. the onset of traveling domains) coincides with the front bifurcation line denoted by the thick solid/dashed curve. For this phase diagram, $a_1 = 2.0$ and $a_0 = -0.1$.

**Figure 19:** Coexistence of traveling and oscillating *periodic* patterns beyond the bifurcation from Ising to Bloch fronts. Both (a) and (b) are obtained for the same computational parameters with different initial conditions. Note the difference in average wavelength between the two patterns. Computational parameters: $\epsilon = 0.013, \delta = 2.5, a_1 = 2.0, a_0 = -0.1$.

**Figure 20:** Front-boundary interactions. (a) Transient domain region: the front is absorbed at the boundary. (b) Stationary domain region: the front is stopped at the boundary. (c) Oscillating domain region: the front oscillates near the boundary. (d) Traveling domain region (beyond the front bifurcation): the front is reflected at the boundaries. All simulations are with Neumann boundary conditions.

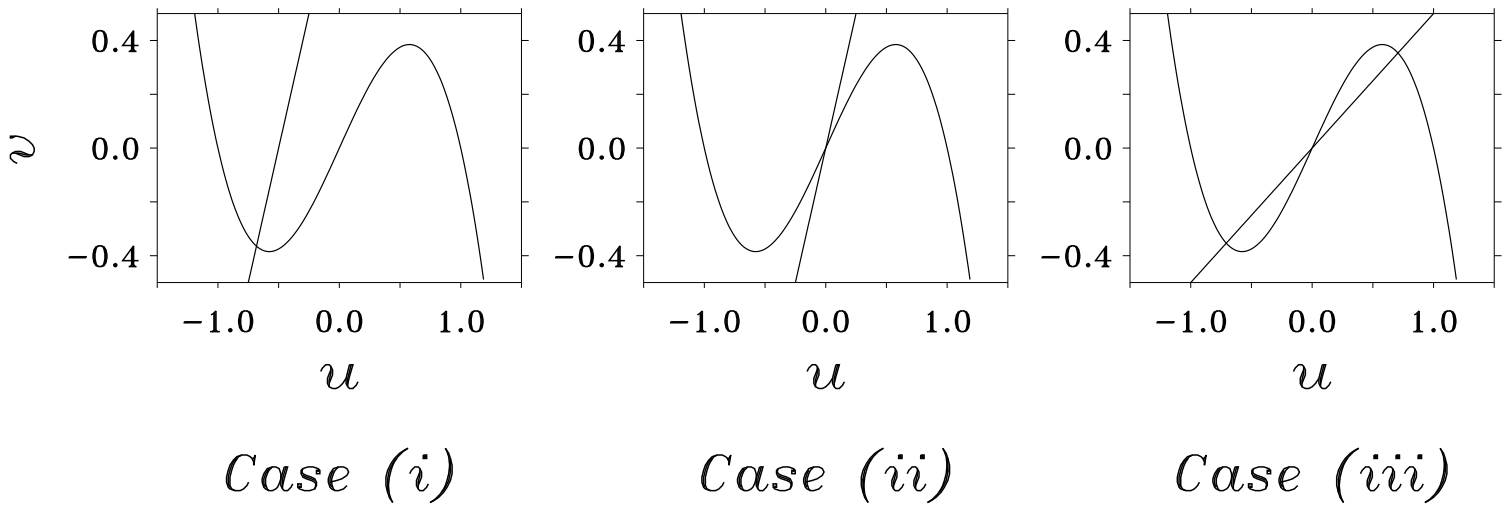


Figure 1: Three basic cases for the nullclines of the model system (1.1). Case (i): The nullclines intersect at a single point on an outer branch of the cubic nullcline. Case (ii): The nullclines intersect at a single point on the middle branch of the cubic nullcline. Case (iii): The nullclines intersect at three points each on a different branch of the cubic nullcline.

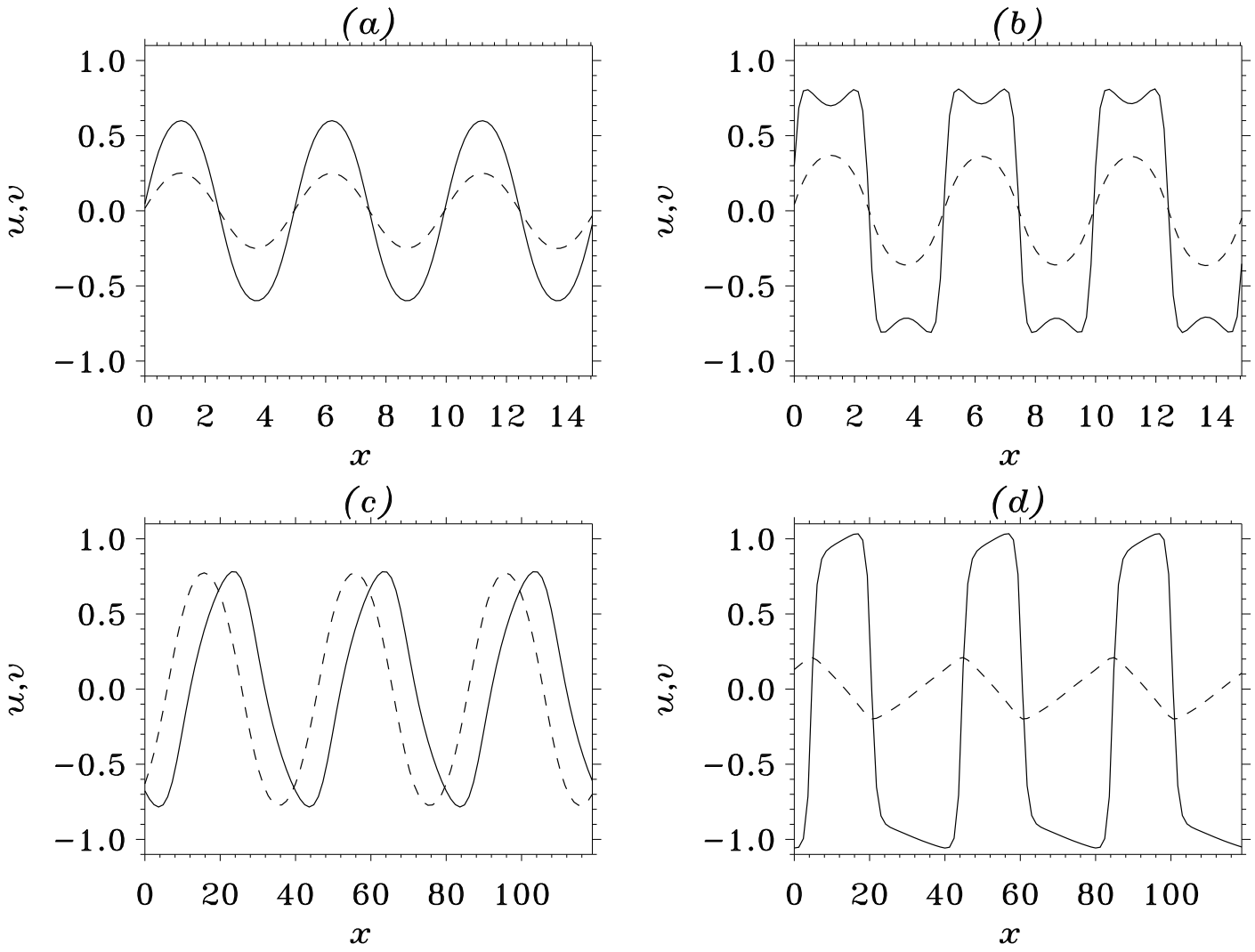


Figure 2: Patterns near and far from onset show the development of two spatial scales. (a) Stationary periodic pattern near onset of the Turing instability. (b) Stationary periodic pattern far from onset of the Turing instability. (c) Traveling pattern near the Hopf bifurcation. (d) Traveling pattern far from the Hopf bifurcation. In all the figures the solid line is the $u$ field and the dashed line is the $v$ field.

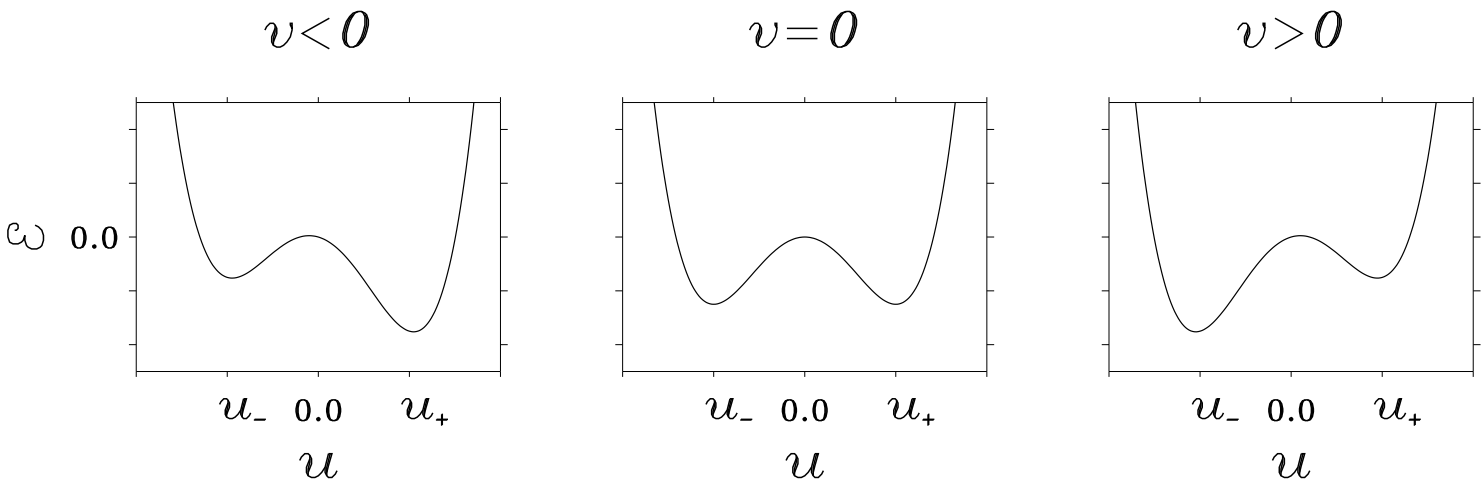


Figure 3: The free energy density $\mathcal{E}$ (see (3.3)) for different values of $v$.

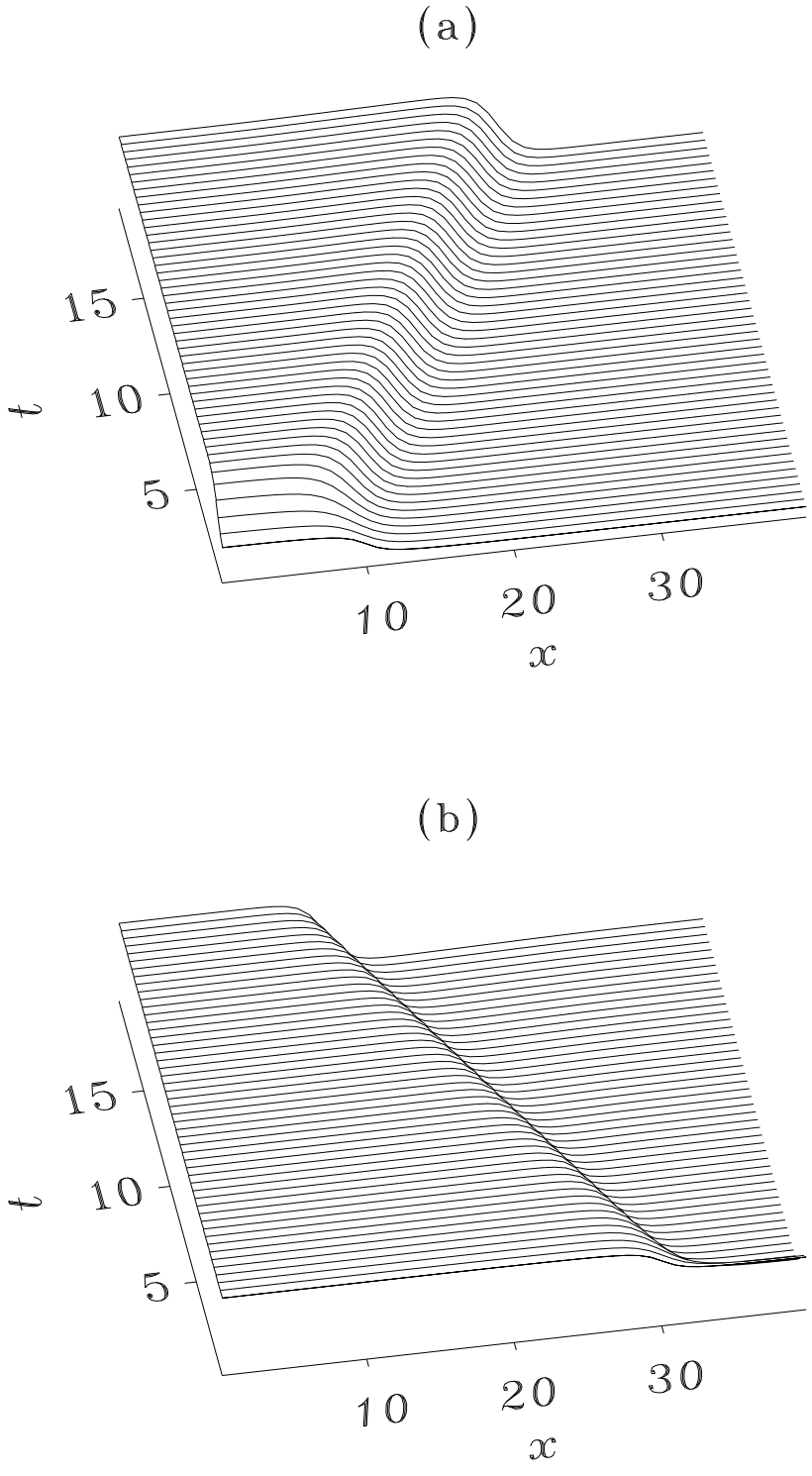


Figure 4: Multiplicity of stable front solutions when $\epsilon \ll 1$. (a) Preparing the system in the down state and perturbing it locally at the left edge of the domain induces a front propagating to the right. (b) Preparing the system in the up state and perturbing it locally at the right edge of the domain induces a front propagating to the left.

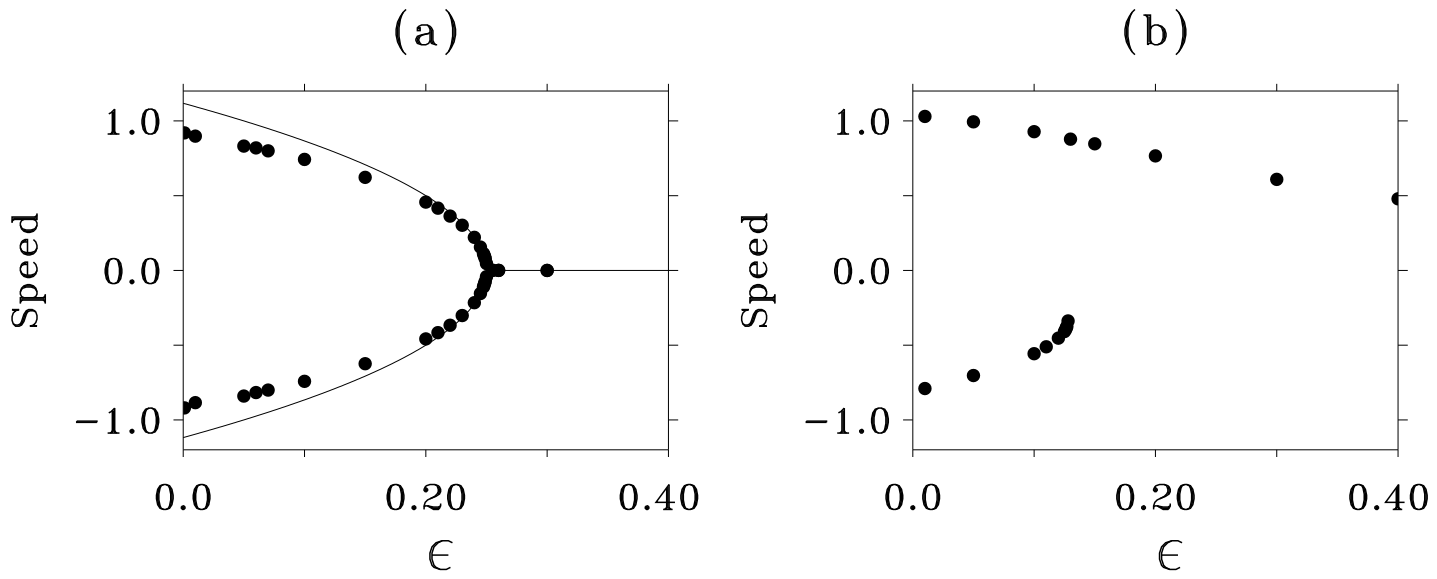


Figure 5: Bifurcation diagrams of front solutions. The dots are data points representing the speed of the different types of stable front solutions that exist for each value of $\epsilon$. (a) The symmetric case ($a_0 = 0$). The solid line is the theoretical bifurcation diagram computed from (3.21). (b) The nonsymmetric case ($a_0 = .1$) shows the unfolding of the pitchfork to a saddle node bifurcation.

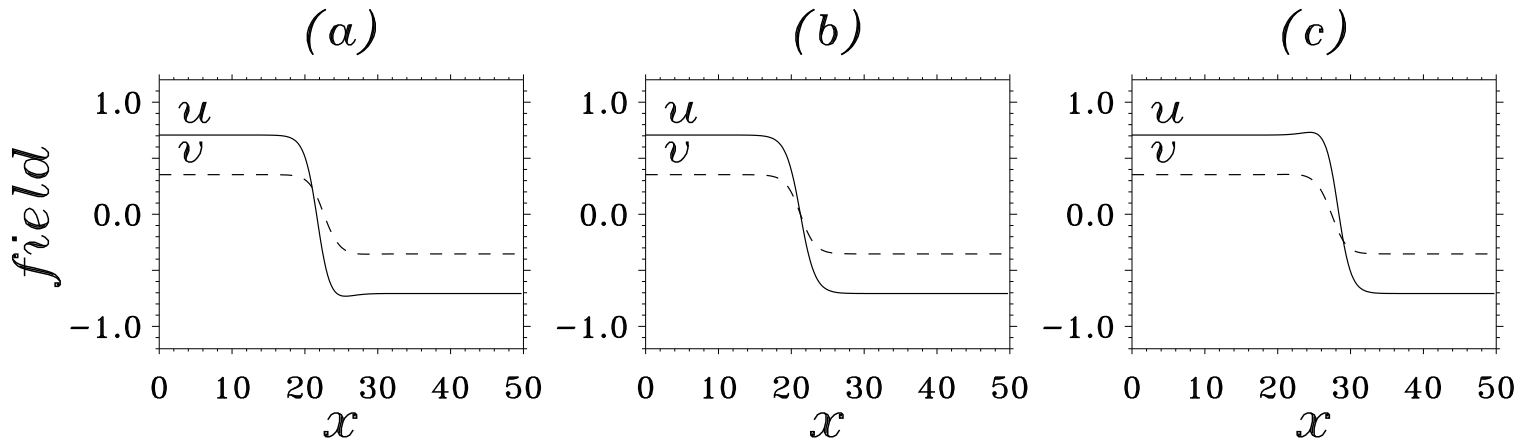


Figure 6: The propogation direction of Bloch fronts is determined by the translation of the $v$ field relative to the $u$ field; $v$ always lags behind $u$ unless the front is stationary. (a) Left traveling front. (b) Stationary front. (c) Right travling front.

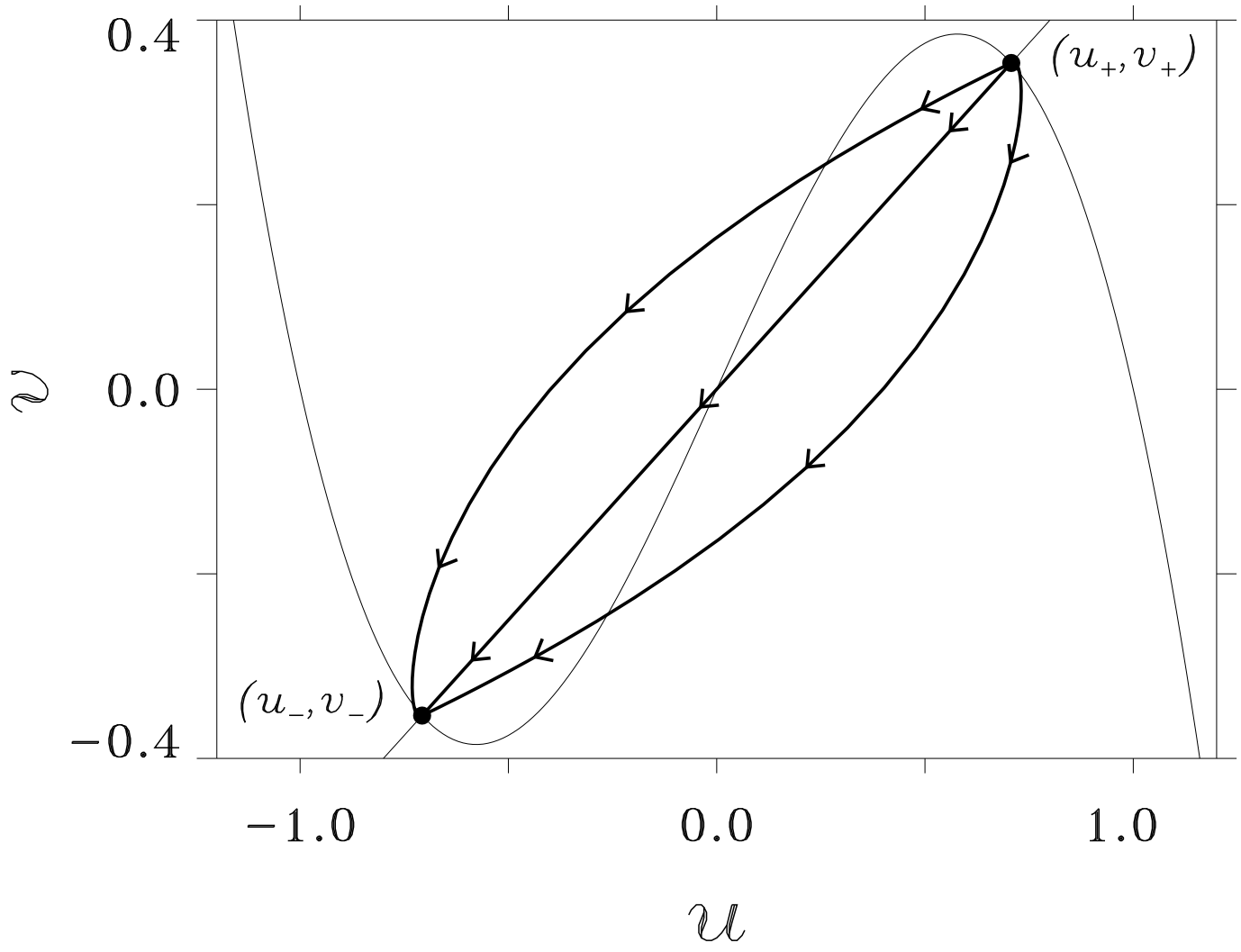


Figure 7: Phase portraits of front solutions connecting the $(u_+, v_+)$ state at $\chi = -\infty$ to the $(u_-, v_-)$ state at $\chi = \infty$ for the symmetric model ($a_0 = 0$) with $\delta = 0$. The light colored curves are the nullclines $f = 0$ and $g = 0$ and the dark colored curves are the numerically computed trajectories. The trajectory through $(0, 0)$ corresponds to the symmetric stationary front solution. The two other trajectories break the odd symmetry of the system and correspond to traveling fronts. The computational parameters are $\epsilon = 1.0, \delta = 0, a_1 = 2.0, a_0 = 0$ for the stationary front and the same with $\epsilon = .2$ for the two traveling fronts.

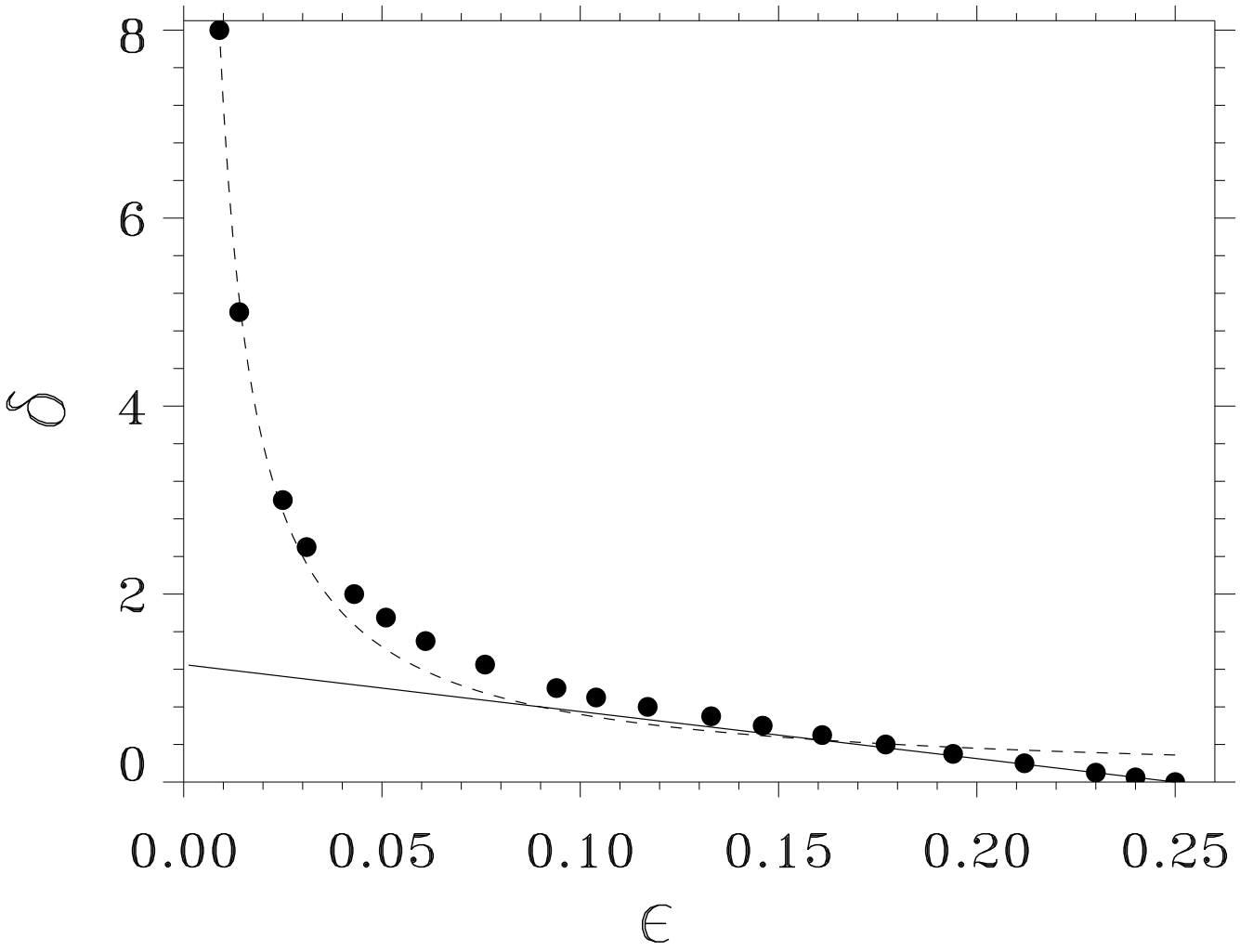


Figure 8: The front bifurcation line in the $\epsilon - \delta$ plane for the symmetric ($a_0 = 0$) model with $a_1 = 2.0$. The solid circles represent the numerically calculated bifurcation line. The solid line is the linear approximation (valid for $\delta \ll 1$) and the dashed line is the singular pertubation result (valid for $\delta/\epsilon \gg 1$).

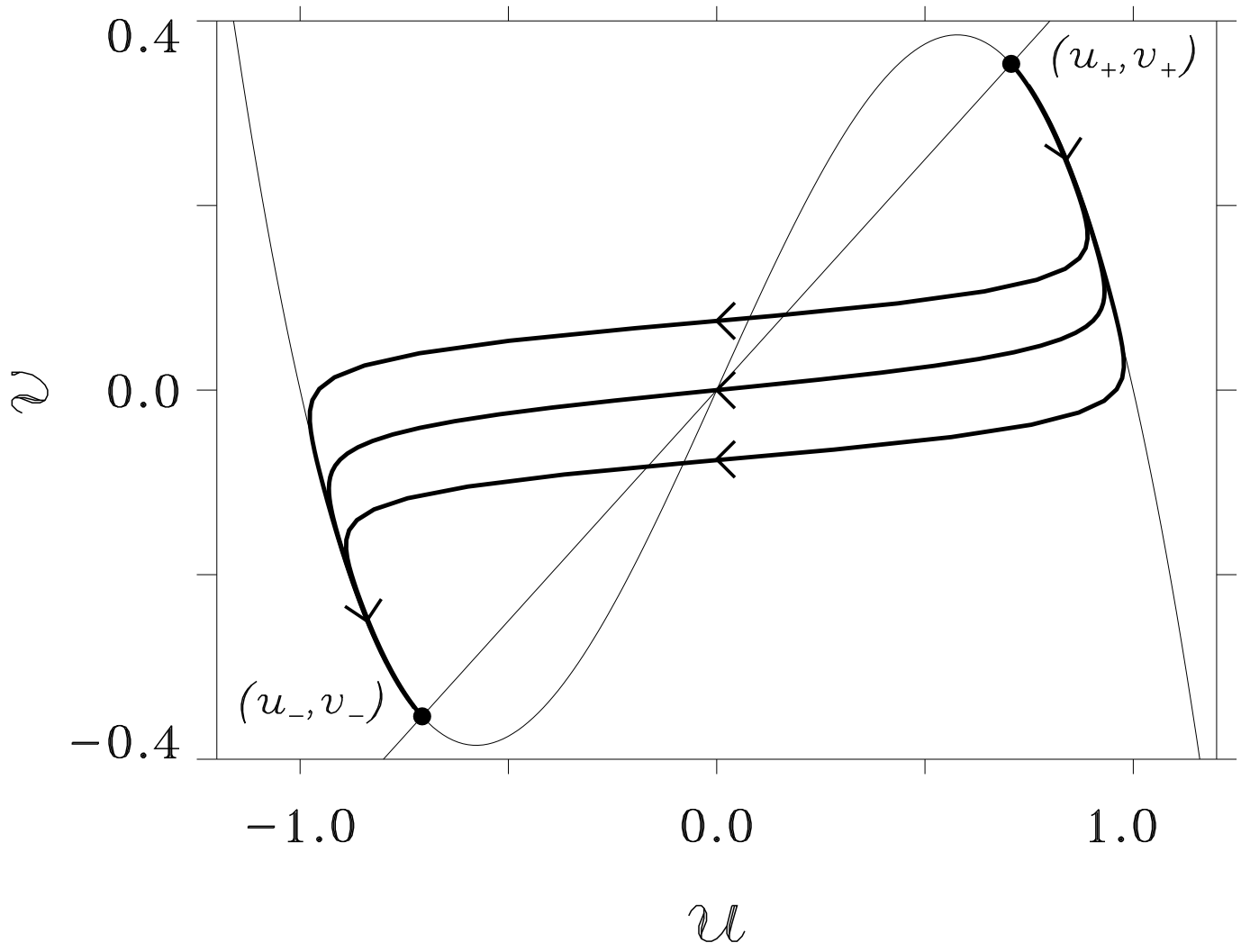


Figure 9: Phase portraits of front solutions connecting the $(u_+, v_+)$ state at $\chi = -\infty$ to the $(u_-, v_-)$ state at $\chi = \infty$ for the symmetric model ($a_0 = 0$) with $\delta > 1$. The light colored curves are the nullclines $f = 0$ and $g = 0$ and the dark colored curves are the numerically computed trajectories. The trajectory through $(0, 0)$ corresponds to the symmetric stationary front with $\epsilon > \epsilon_c(\delta)$ and the two other trajectories correspond to the symmetry breaking traveling fronts with $\epsilon < \epsilon_c(\delta)$.

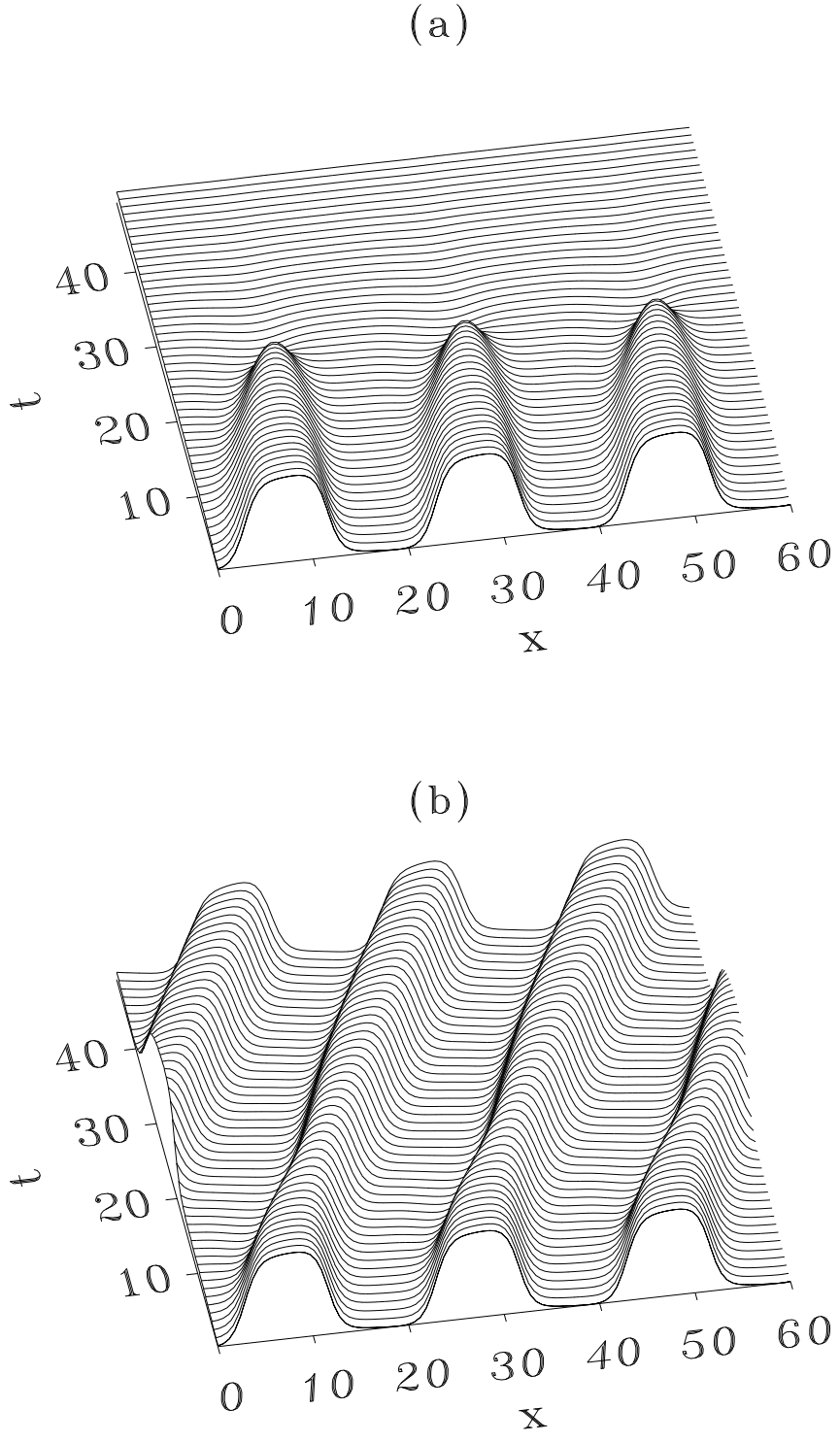


Figure 10: (a) Relaxation of an initial pattern to the uniform down state for the regime of Ising fronts, $\epsilon = 0.14, \delta = 0, a_1 = 2.0, a_0 = -0.1$. (b) The convergence of the same initial pattern toward a stable traveling pattern beyond the bifurcation from Ising to Bloch fronts, $\epsilon = 0.09$.

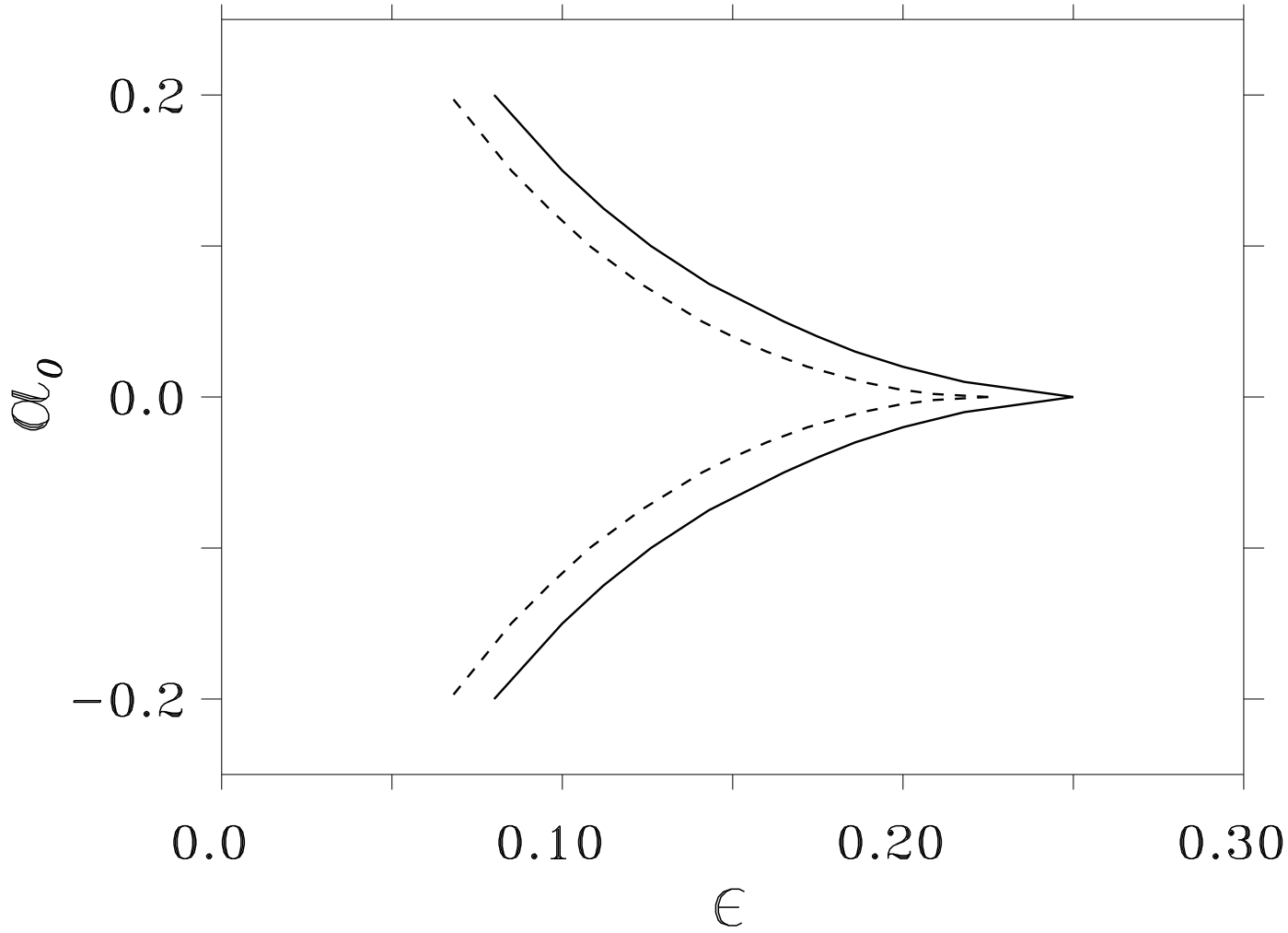


Figure 11: Phase diagram in the $\epsilon - a_0$ plane. For the region to the right of the solid curve only one type of front solution exists and initial patterns do not persist. In the region between the solid and the dashed curves multiple stable fronts coexist but patterns still decay toward a uniform state. For the region to the left of the dashed curve initial patterns evolve toward persistent patterns in the form of stable traveling waves. Computational parameters are : $\delta = 0,\ a_1 = 2.0$.

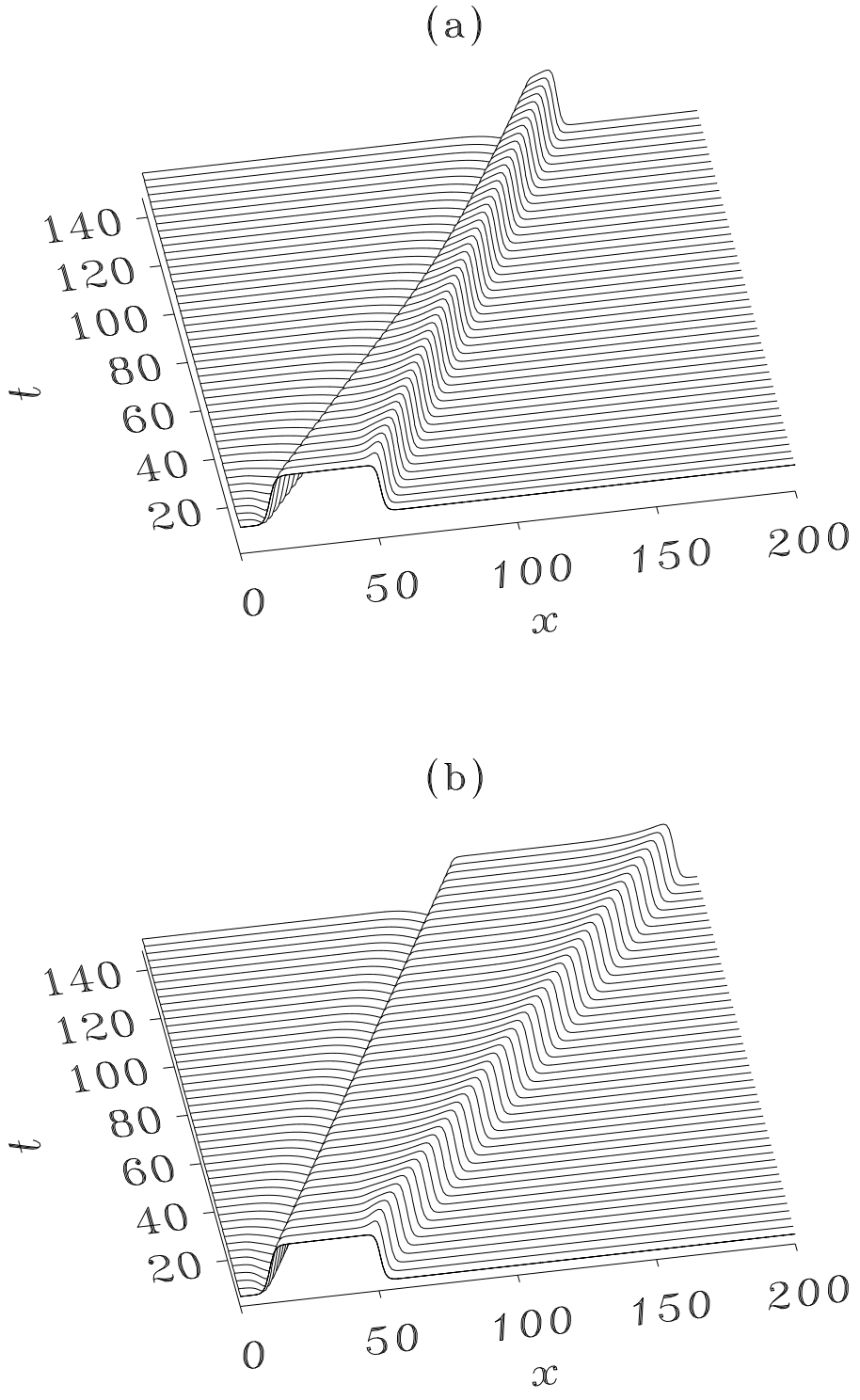


Figure 12: Time evolution of a front and a back (or two Bloch fronts following one another). (a) The back propagates faster than the front and binds to the front to form a traveling up state domain. (b) The back propagates slower than the front and the up state domain expands indefinitely.

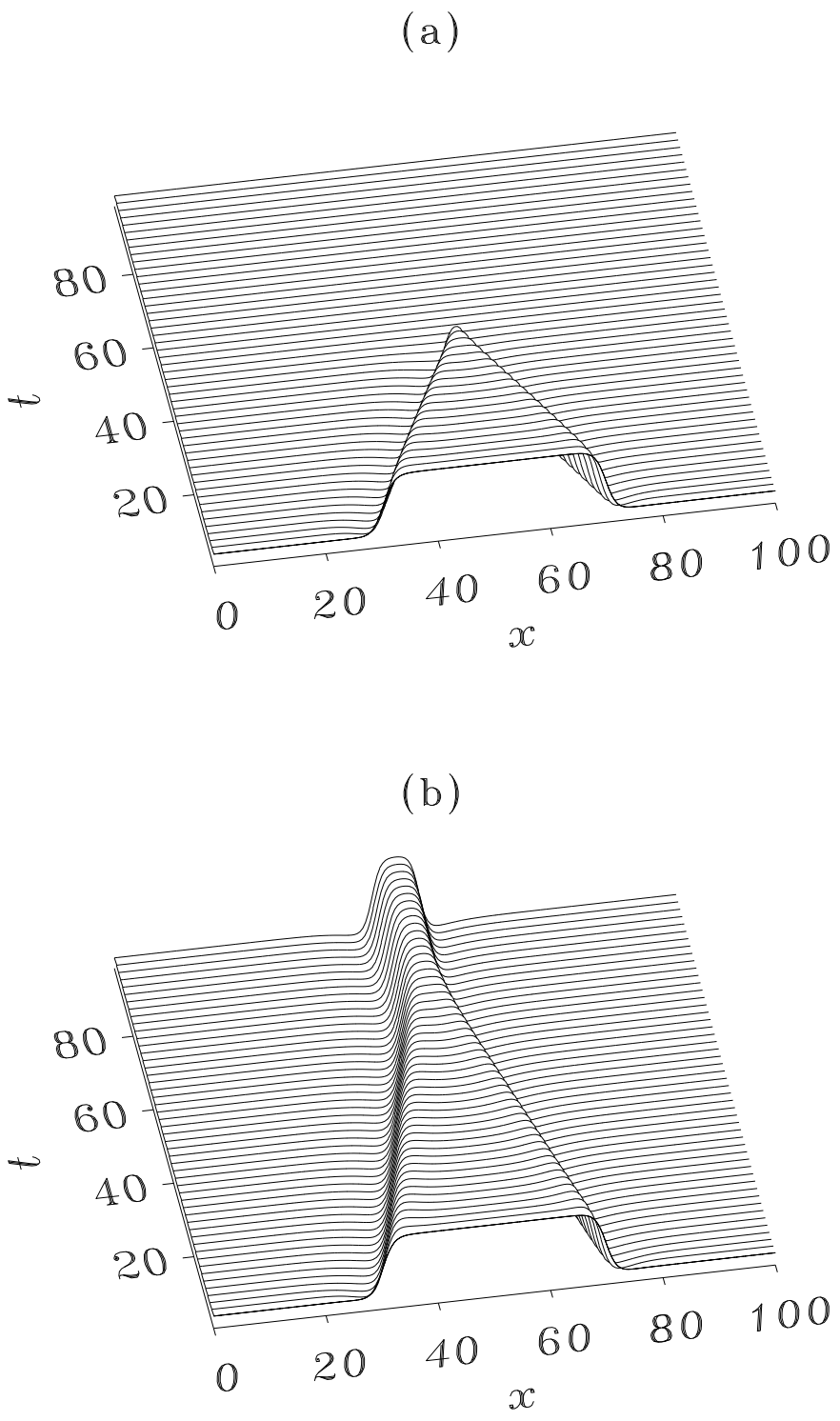


Figure 13: The onset of stationary domains in the Ising front regime as $\delta/\epsilon$ is increased. Ising fronts either (a) collide and anihilate to form a uniform state for $\epsilon > \mu_{st}\delta$, or (b) slow to a stop and form a stationary domain for $\epsilon < \mu_{st}\delta$.

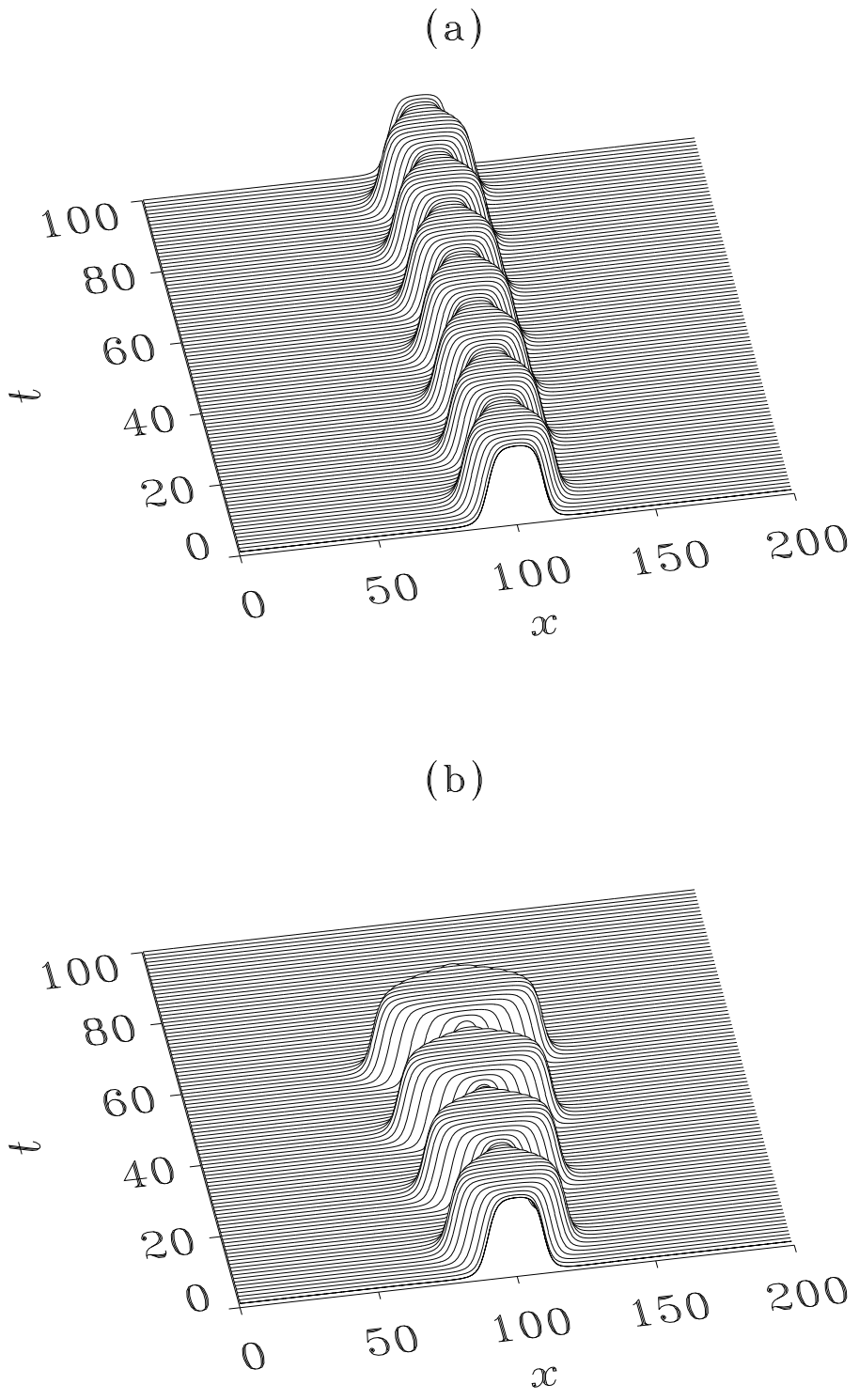


Figure 14: Oscillating or breathing domains. (a) Steady oscillations close to the Hopf bifurcation. Computational parameters $\epsilon = 0.03, \delta = 2.5, a_1 = 2.0, a_0 = -0.1$. (b) Collapse of an oscillating domain further away from the Hopf bifurcation. Compuational parameters are the same with $\epsilon = 0.025$.

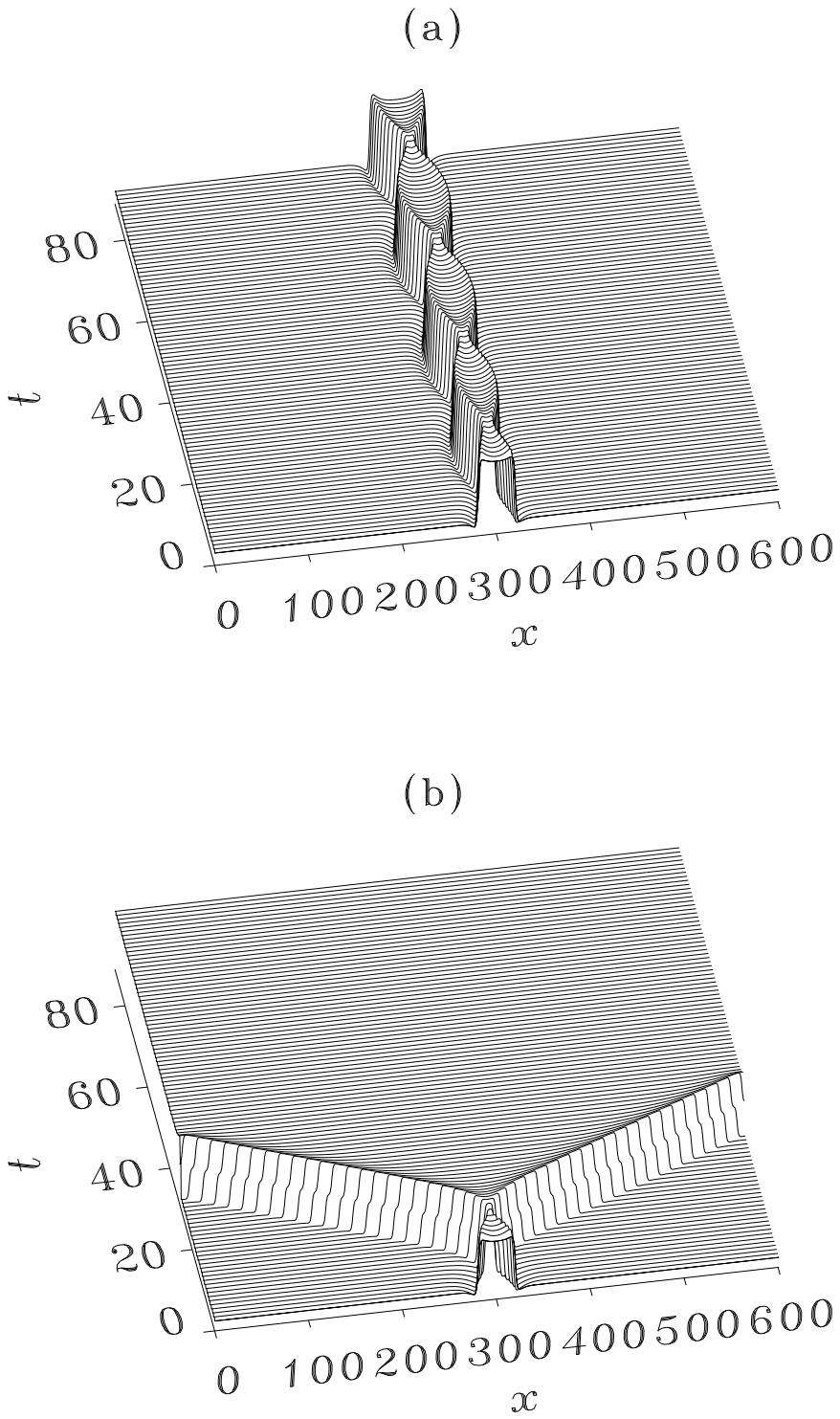


Figure 15: The effect of the front bifurcation on the dynammics of two fronts propagating toward one another: (a) Below the bifurcation ($\epsilon > \epsilon_c(\delta)$ an oscillating domain is formed. Computational parameters: $\epsilon = 0.03, \delta = 2.5, a_1 = 2.0, a_0 = -0.01$. (b) Beyond the bifurcation the two fronts rebound from one another and propagate to the boundaries. Same parameters as in (a) except that $\epsilon = 0.012$.

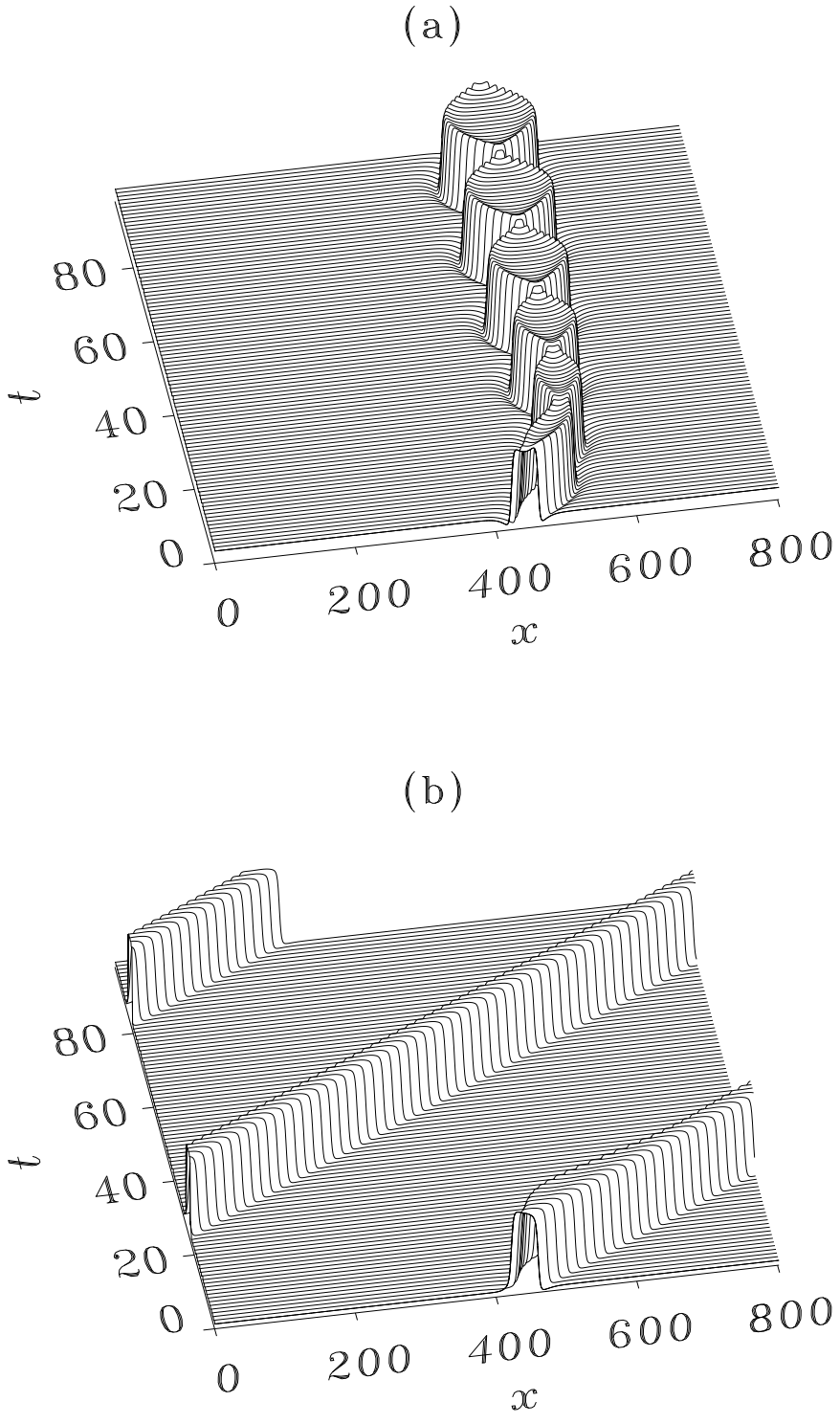


Figure 16: The effect of the front bifurcation on the dynamics of two fronts following one another: (a) Below the bifurcation ($\epsilon > \epsilon_c(\delta)$) an oscillating domain is formed. Computational parameters are $\epsilon = 0.030, \delta = 2.5, a_1 = 2.0, a_0 = -0.012$. (b) Beyond the bifurcation a traveling domain is formed. Same parameters as in (a) except that $\epsilon = 0.25$.

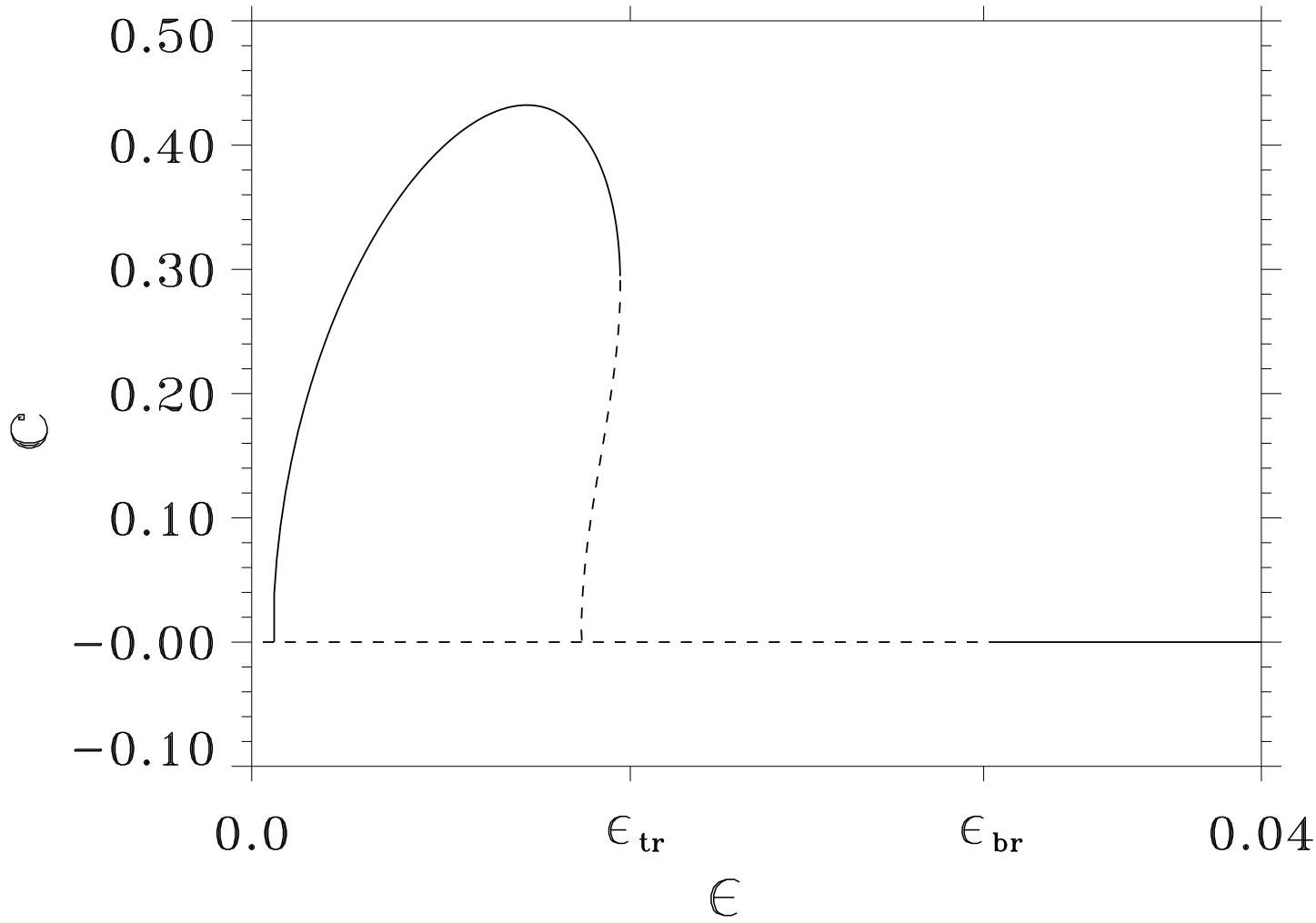


Figure 17: A typical bifurcation diagram for single domain structures. The solutions shown with the solid (dashed) line are stable (unstable) structures. The stationary domain solution loses stability to an oscillating domain at $\epsilon = \epsilon_{br}$. At $\epsilon = \epsilon_{tr}$, a branch of stable traveling domain solutions appears. By the symmetry $c \to -c,\ \chi \to -\chi$, this diagram is symmetric with respect to the $c = 0$ axis, but only the positive speed branch of traveling domain solutions is shown. Also, there is an additional branch of zero speed solutions that is unstable for all values of $\epsilon$. Parameters: $\delta = 2.5, a_1 = 2.0, a_0 = -.1$, period $= 100$.

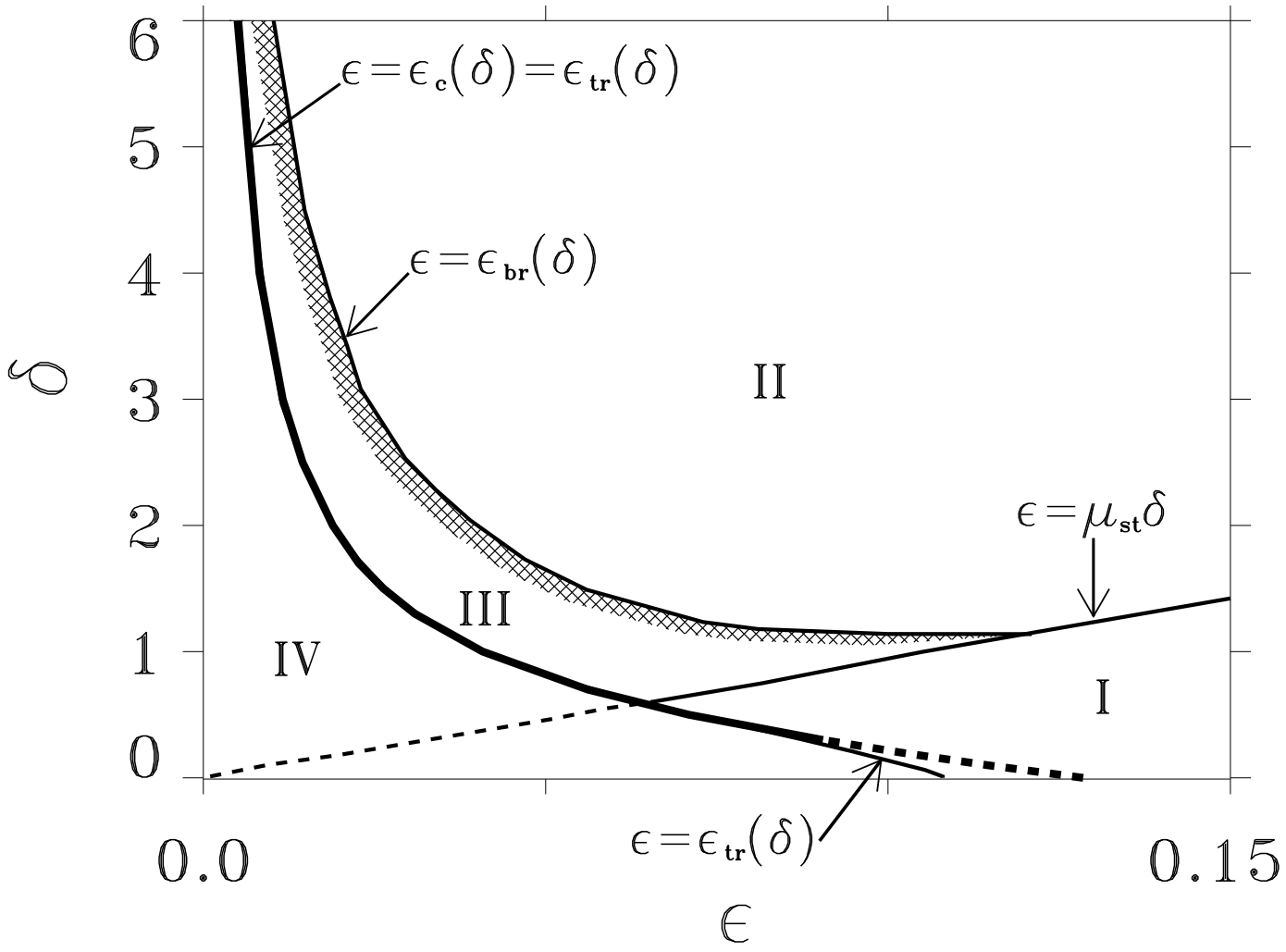


Figure 18: Phase diagram for single domain structures in the $\epsilon - \delta$ plane. In region I, domain structures are transient and the asymptotic state is either the uniform up or down state. In region II stable stationary domains coexist with the uniform up and down states. In region III domains oscillate with a typical region of steady oscillations denoted by the hatched area. In region IV domains travel. The boundary between regions III and IV (i.e. the onset of traveling domains) coincides with the front bifurcation line denoted by the thick solid/dashed curve. For this phase diagram, $a_1 = 2.0$ and $a_0 = -0.1$.

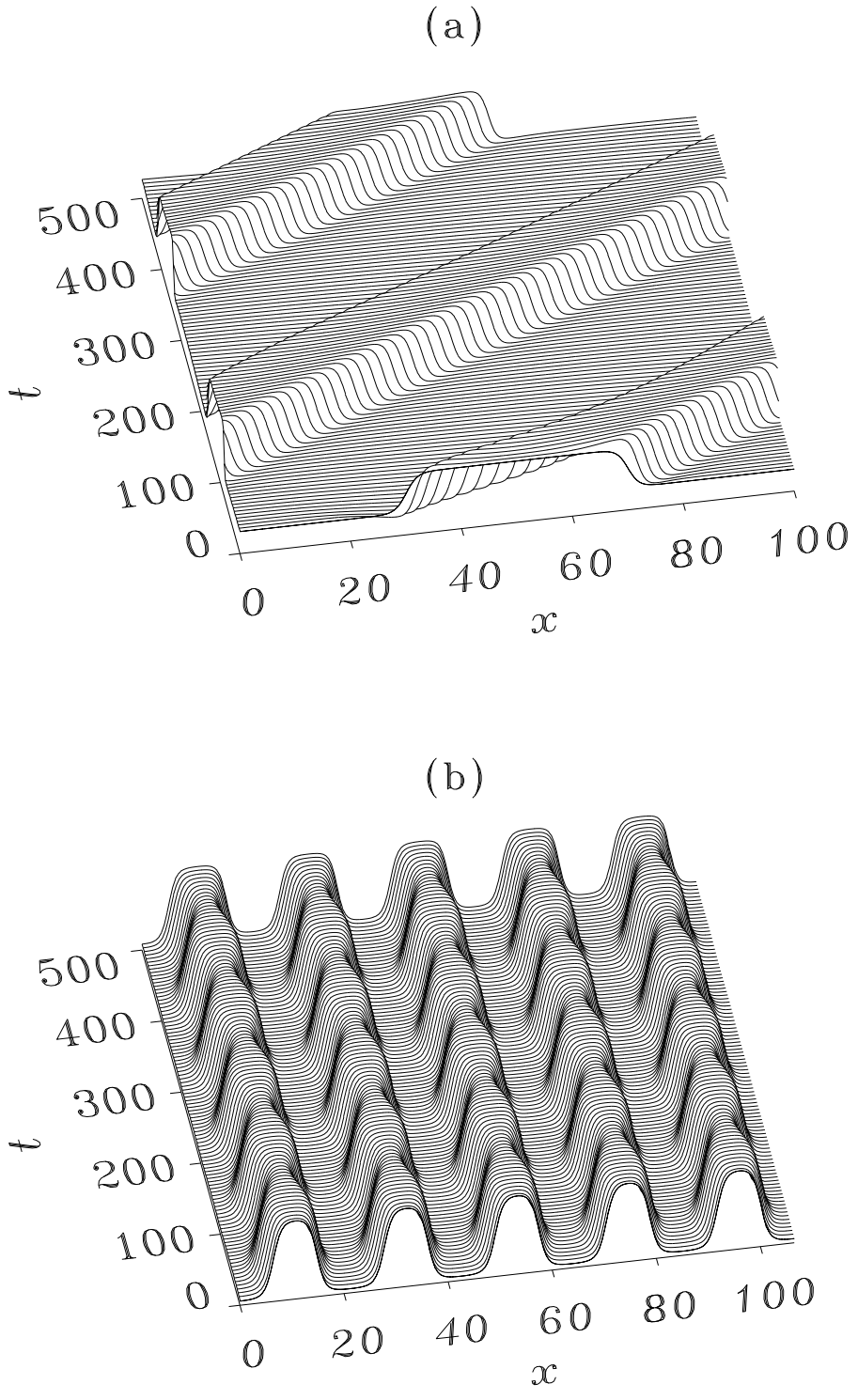


Figure 19: Coexistence of traveling and oscillating *periodic* patterns beyond the bifurcation from Ising to Bloch fronts. Both (a) and (b) are obtained for the same computational parameters with different initial conditions. Note the difference in average wavelength between the two patterns. Computational parameters: $\epsilon = 0.013, \delta = 2.5, a_1 = 2.0, a_0 = -0.1$.

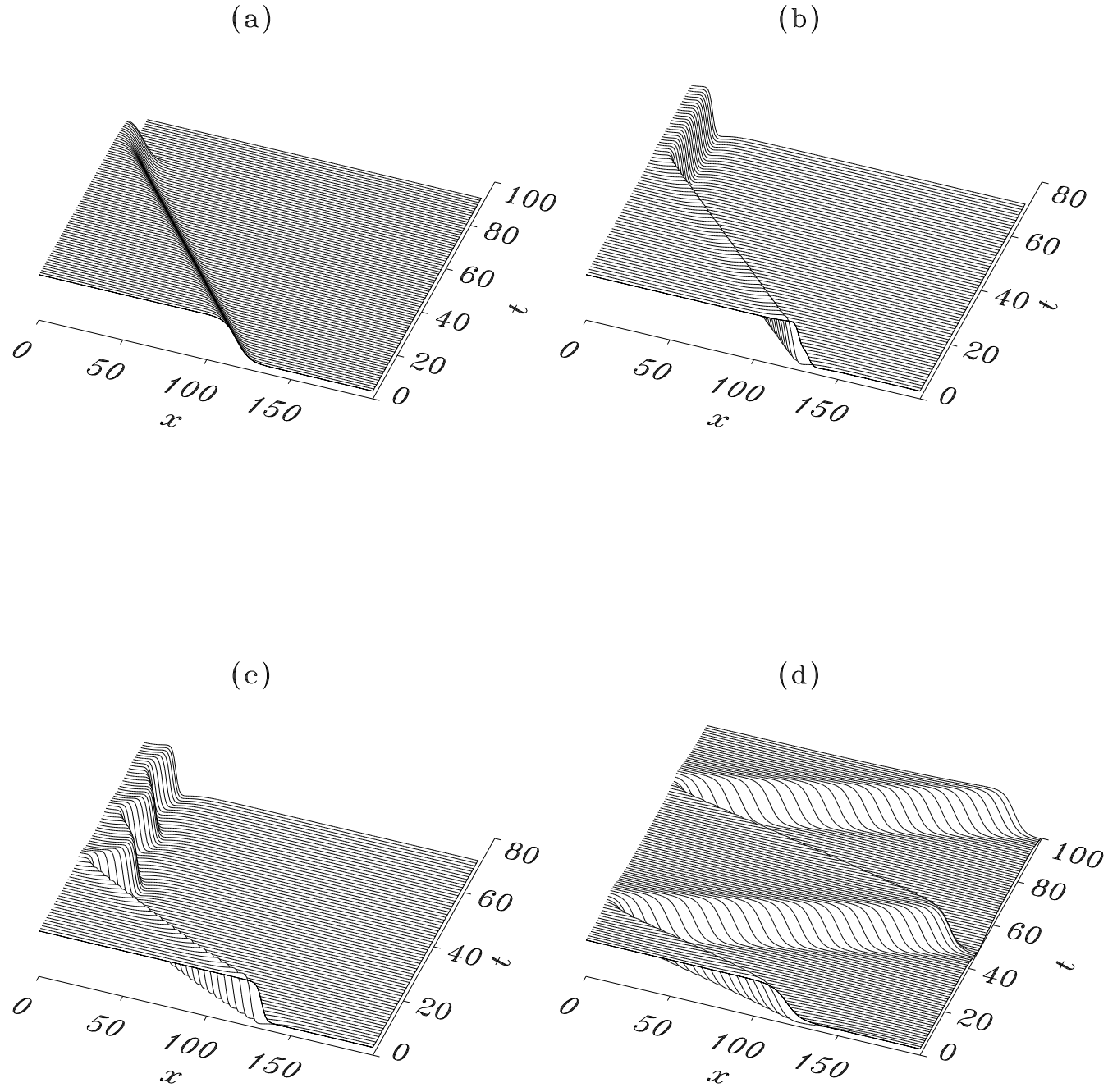


Figure 20: Front-boundary interactions. (a) Transient domain region: the front is absorbed at the boundary. (b) Stationary domain region: the front is stopped at the boundary. (c) Oscillating domain region: the front oscillates near the boundary. (d) Traveling domain region (beyond the front bifurcation): the front is reflected at the boundaries. All simulations are with Neumann boundary conditions.